www.mycoordinates.org

Coordinates

Volume XVIII, Issue 4, April 2022

THE MONTHLY MAGAZINE ON POSITIONING, NAVIGATION AND BEYOND

LiDAR in oil palm disease detection

Spatial and economic inequities and trends in South Africa

In this issue

Articles

Columns

Food insecurity

Extreme climate events and many conflicts

Cause the upward trend in hunger

Even before the pandemic.

And as the pandemic was not enough,

The war has added to the miseries.

High energy prices, high fertilizers prices,

Disruption in supply chain and trades,

All lead to elevated inflation in food prices,

That is further worsened by the reduced income.

Many more millions are slipped into food insecurity

In many parts of the world.

A glaring crisis staring at us!

Bal Krishna, Editor
bal@mycoordinates.org

LiDAR in oil palm disease detection

It can be concluded from this study that TLS remote sensing data provide precise physical properties of oil palm trees

Nur Azuan bin Husin, PhD

Senior Lecturer, Department of Biological and Agricultural Engineering Young Research Associate, Smart Farming Technology Research Center (SFTRC), Faculty of Engineering Universiti Putra Malaysia Selangor, Malaysia

Siti Khairunniza Bejo, PhD

Senior lecturer, Department of Biological and Agricultural Engineering Faculty of Engineering Universiti Putra Malaysia Head SMART Farming Technology Research Centre, Faculty of Engineering Universiti Putra Malaysia Selangor, Malaysia

Introduction

Light Detection and Ranging (LiDAR) is an active remote sensing technique that uses laser light, can be used to produce high-resolution scans of a tree's morphology, often known as plant phenotyping. Laser scanning is a technique for acquiring data that uses the LiDAR principle. The laser scanner, also known as 3-D laser imaging, is a device that is used to capture, collect, and store precise data of an object's physical size and shape. Laser scanners work on the idea of producing laser light that hits an object and then reflects back to the scanner. The data is then transferred to a computer and shown as a digital three-dimensional model. The laser scanner able to scan object's surface rapidly then record the shape and visual properties in form of intensity and/or RGB information. The collected information is returned to the unit in the form of point cloud data that consists of XYZ coordinates. It was designed to capture accurately on smaller objects for inspection, replication and other purposes. There are various types of laser scanners, including mobile, airborne, and terrestrial scanning. The mobile laser scanner (MLS) was designed to work from a moving vehicle, such as a car, boat, train, or other similar vehicles. Aerial scanning, also known as airborne laser scanning (ALS), is carried out using an unmanned aerial vehicle (UAV), planes, or helicopters. It usually involves mapping and terrain surveys over a large area. Terrestrial laser scanning (TLS) is a ground-based version of the airborne LiDAR is an accurate, quick and flexible measurement technique that can complement or partially replace other existing geodata acquisition technologies. Currently, there are three types of laser scanner namely time of flight (TOF) scanner, phase-shift (PS) scanner and triangulation-based system scanner.

Previous research yielded high correlation and accuracies indicates that LiDAR technology can be used in the agricultural field and possible to be applied in the oil palm plantation for BSR disease detection. A tree's biophysical features can be assessed to determine whether it was infected with a specific disease or related pathological disorders associated with distinctive symptoms. Because of the infection, there were differences in canopy density between healthy and infected trees, with infected trees having reduced foliage density and leaf area. The 3D canopy structure model was used to analyse vegetation diseases, and it was discovered that disease severity was associated with a canopy structure. In addition, because the disease affects crop morphology and canopy structure, it can be recognised early by observing changes in canopy morphology. Furthermore, canopy biophysical parameters, canopy structure, and geometry are critical in predicting the healthiness of the canopy. This article discusses briefly the previous study on the application of LiDAR for Basal Stem Rot (BSR) disease in oil palm plantation, consisting of changes in oil palm architecture, stratification of oil palm crown, combination of parameters and machine learning approach and multi temporal study.

The most threatening disease to the oil palm is Basal Stem Rot (BSR) disease caused by *Ganoderma boninense*. The main canopy symptoms of BSR disease are

declination of the tree's canopy forming a "skirt-like" shape, appearance of unfolded spears and smaller crown size because of leaves deterioration. All these physical symptoms are progressing gradually from mild to severe level. Thus, the level of infection can be classified. Therefore, in these studies, oil palm trees were categorised into four health levels - T0, T1, T2 and T3, which represents the healthy, mildly infected, moderately infected and severely infected, respectively based on the symptoms of BSR disease. The TLS scanner was mounted at a height of 1 m at a distance of 1.5 m and each palm was

scanned at four scan positions around the tree to get a full 3D image. All collected scans were imported into SCENE software for processing and further analysis. The "Registration" step was completed in order to match the multiple scan positions and to synchronise the laser point data to create a cluster of point clouds.

Oil palm canopy architecture

Three parameters were investigated in the research of oil palm canopy architecture: the number of pixels inside the crown

(crown pixel), the degree of angle between fronds (frond angle), and the number of fronds (frond number). The findings reveal that the crown pixel, frond angle, and frond number are all significantly related and that the BSR severity levels are highly correlated. As a result, the mildly infected (T1) stage of a *Ganoderma boninense* was the earliest stage that could be detected. For frond angle, all post hoc tests showed consistent results, and all levels were significantly separated except for T0 and T1. By using the crown pixel parameter, healthy trees (T0) were separated from unhealthy trees (moderate infection [T2] and severe infection [T3]. Using the crown pixel and frond angle data, *Ganoderma boninense* could be diagnosed as early as the T2 level. It is difficult to tell the difference between T0 and T1 because the symptoms are so similar with a moderate infection.

In the study of oil palm canopy architecture, three parameters were analyzed: number of pixels inside the crown (crown pixel), the degree of angle between fronds (frond angle), and the number of fronds (frond number). The
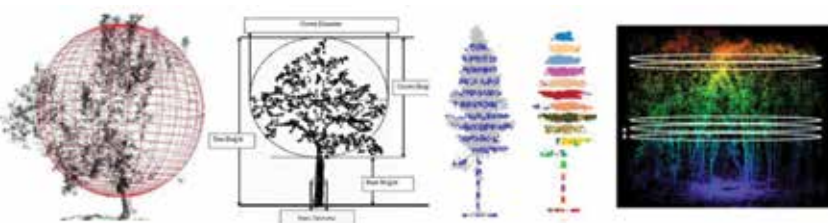
Fig. 1. LiDAR for crown trees' characteristics
Source: Moorthy et al. (2011); Pratihast (2010); Yang et al. (2016); Trochta et al. (2016)
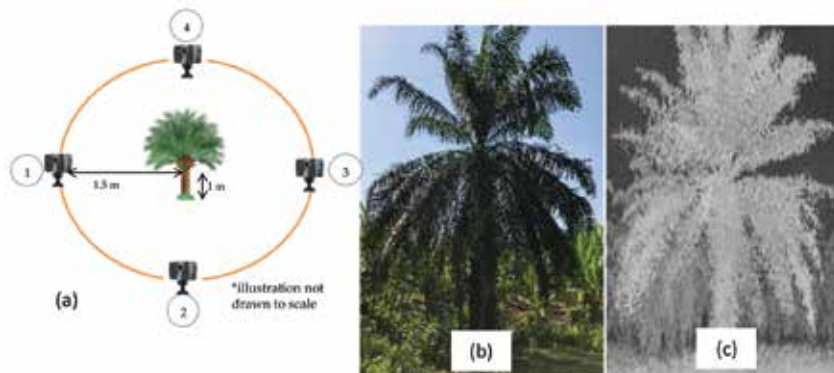
Fig. 2. (a) Data collection setup; (b) Oil palm tree; (c) Oil palm's point cloud image
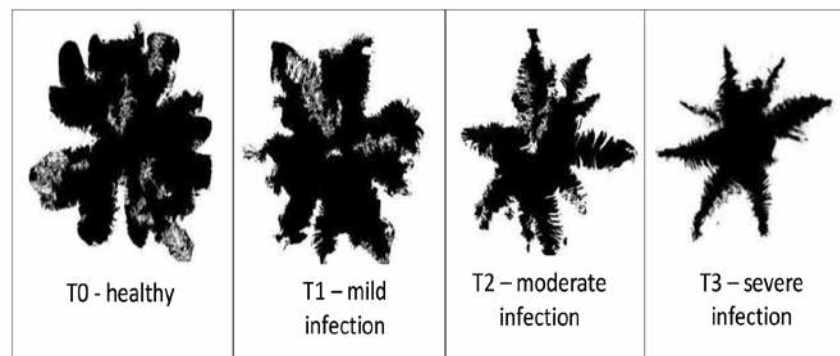
Fig. 3. Examples of crown top view images for each healthiness level
Source: Azuan et al. (2019)

The use of physical features of the canopy structure in this novel image processing technique is critical for early disease identification, management, and control. With the help of preprocessing and postprocessing facilities, it also can be employed for in situ application.

Fig. 4. The descriptions of canopy stratification method.
Source: Husin et al. (2010)

Fig. 5. Schematic of the method used for parameters extraction.
Source: Husin et al. (2020)
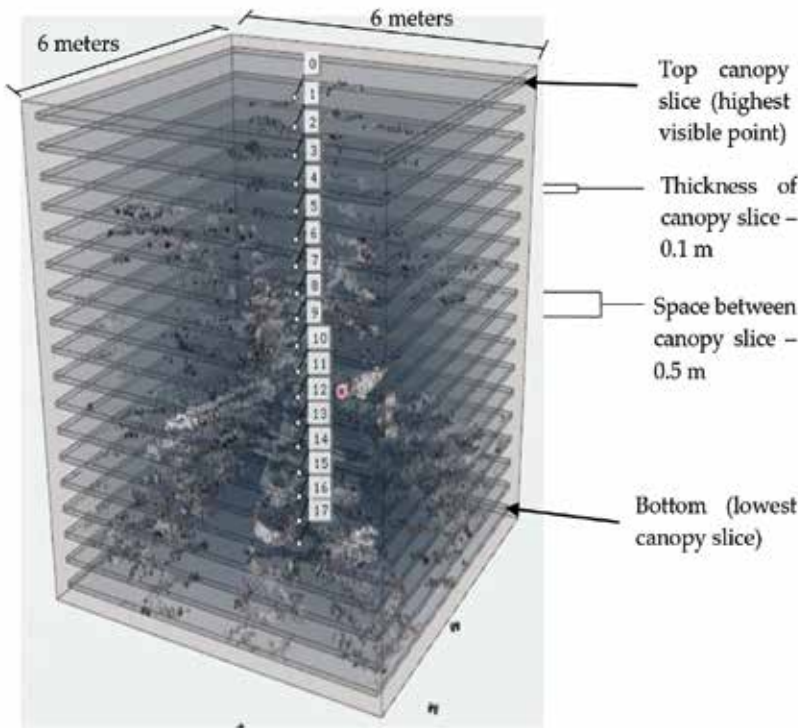
results show that the crown pixel, frond angle, and frond number are significantly related and that the BSR severity levels are highly correlated. Therefore, the earliest stage that a *Ganoderma boninense* could be detected was mildly infected (T1). For frond angle, all post hoc tests showed consistent results, and all levels were significantly separated except for T0 and T1. By using the crown pixel parameter, healthy trees (T0) were separated from unhealthy trees (moderate infection [T2] and severe infection [T3]. Thus, *Ganoderma boninense* could be detected as early as the T2 level by using the crown pixel and the frond angle parameters. It is hard to differentiate between T0 and T1, because during mild infection, the symptoms are highly similar.

Stratification of oil palm crown

This study used TLS data to examine the effect of crown profile due to BSR and develop a BSR detection model using crown strata. The crown stratification method was used to create crown strata (referred to as Cn; where n is the crown length in cm). The amount of laser hits in the strata was used to create crown profiles comparing healthy and diseased oil palm trees, establish prediction models, and evaluate crown density trends in different regions of the tree. By using a systematic multi-scan approach, the study was able to account for the occlusion issue. The profiles of crown strata revealed that the healthy trees have higher crown densities than unhealthy trees starting from 250 cm from the top (strata no. 5) to the bottom. In the classification of healthy and infected trees, prediction models based on the strata parameters C650, C700, C800, and C850 were 92.5 per cent accurate.

Combination of parameters and machine learning approach

Five parameters were analysed: canopy strata at 200 cm from the top, canopy strata at 850 cm from the top), crown pixel
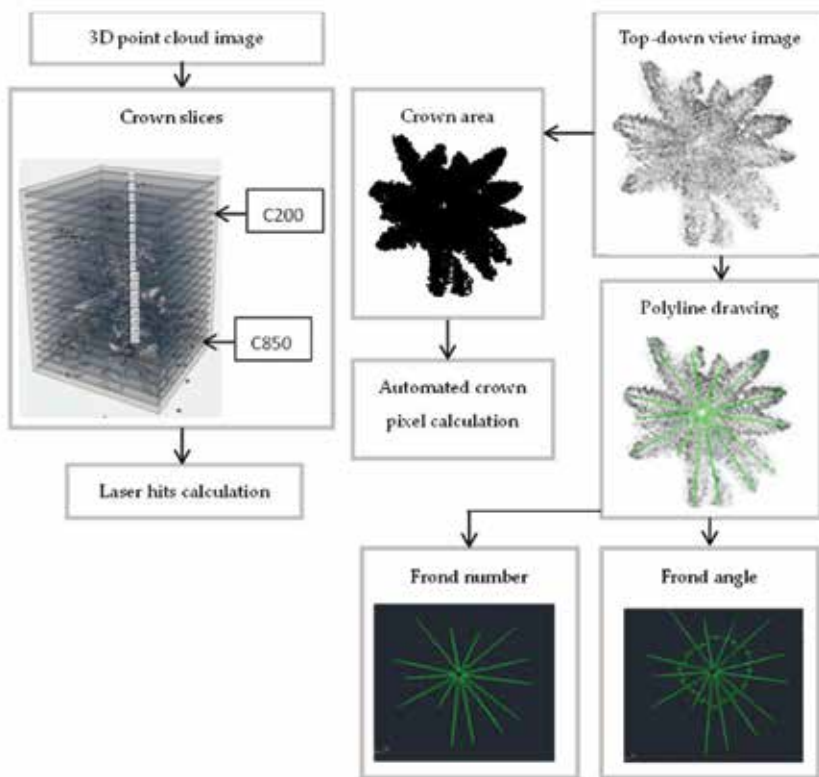
> The proposed method's key flaw is the feature extraction process, as some of the characteristics required to be manually extracted. The extraction of features could be automated in the future using deep learning technology.

(number of pixels inside the crown), frond angle (degree of angle between fronds) and frond number. According to statistical analysis, the best single parameter for detecting BSR illness as early as T1 was frond number. In classification models, a linear model with a combination of parameters, ABD – A (frond number), B (frond angle), and D (S200) produced the highest average accuracy for categorization of healthy-unhealthy trees, with an accuracy of 86.67 per cent. It also can classify the four categories of infection severity with an accuracy of 80%. When compared to the severity categorization based on frond number, this model performed better. This model performed better when compared to the severity classification using frond number.

The aforementioned parameters were evaluated using principal component analysis (PCA) in a machine learning approach to minimise the dimensionality of the dataset and increase its interpretability while minimising information loss. The results showed that the kernel naïve Bayes (KNB) model developed using the input parameters of the principal components (PCs) 1 and 2 had the best performance among 90 other models with a multiple level accuracy of 85% and a Kappa coefficient of 0.80. Furthermore, the classification success was aided by the combination of the two largest PC variances with the most weighted to frond number, frond angle, crown area, and C200. The model was also 100 per cent accurate in classifying healthy and mildly infected trees.

Multi temporal study

In the precision agriculture field, spatio-temporal data is critical for better oil palm management. It can be done by understanding disease development for long-term solutions, and providing a quick response so that suitable treatment may be delivered to the palm as soon as feasible. With two distinct scan lengths, i.e. 2- and 4-months following the first scan, terrestrial laser scanning data was used to analyse changes in the crown and frond metrics of oil palm plants. To evaluate significant differences in the parameters at different times in time, statistical analyses were performed, including the Kruskal–Wallis test with $\alpha = 0.05$ and the Wilcoxon post-hoc test. The crown strata number 17 (850 cm from the top) and the crown area were found to be the most appropriate criteria to utilise. Furthermore, by comparing the 4-month scan with the second 2-month scan, oil palm trees with BSR can be identified. The findings revealed that the effects of *Ganoderma boninense* infection can be distinguished at the later stage.

Conclusion

It can be concluded from this study that TLS remote sensing data provide precise physical properties of oil palm trees. The work filled a research gap in the application of TLS in oil palm disease detection research. The terrestrial laser scanner's extensive laser point data can be used to identify the geometric aspects of oil palm plants. The use of physical features of the canopy structure in this novel image processing technique is critical for early disease identification, management, and control. With the help of preprocessing and postprocessing facilities, it also can be employed for in situ application. TLS delivers tree-level data to help farmers achieve their precision farming goals. The laser scanner will give faster scanning times and more broad scanning coverage for the entire plantation in the future. A sensing system based on cutting-edge algorithms and onsite technology could provide more precise data for establishing an up-to-date oil palm plantation health database.

Despite its potential, the proposed method's key flaw is the feature extraction process, as some of the characteristics required to be manually extracted. The extraction of features could be automated in the future using deep learning technology. Meanwhile, the plantation manager could examine the position and healthiness level of the trees via an online platform, and an alert system might be built. Furthermore, by taking into account the differences in static and dynamic systems, such as spatial resolution, viewing angle, scanning area, distance, scanning mechanism, data capture mode, and the obtainable accuracy, the method could be expanded by using mobile laser scanning (MLS) and airborne laser scanning (ALS). The scans might be done concurrently in MLS by attaching the mobile scanner to a trailer or tractor employed in the plantation, with a clear path and clear height in the plantation planned to avoid colliding with the fronds. Meanwhile, ALS has the potential to cover a bigger area and take less time than TLS.

LiDAR data is becoming more widely available and of higher quality, and when combined with a method for identifying individual oil palm trees, it has the potential to be useful in research and precision agriculture applications. TLS' availability and resolution are anticipated to rise as technological advances continue. Scanners with advanced and greater capability, capable of scanning an entire plantation area with a single scan at a reduced cost, could be created in the future. The method might be used to create an accurate and quick oil palm health map for disease identification in real-time.

Spatial and economic inequities and trends in South Africa

It paper aims to better understand the spatial interlinkages between racial segregation, poverty, household composition, land value and income inequality in these areas

Sue Bannister
Director, City Insight
(Pty) Ltd
South Africa

Dr Michael Sutcliffe
Director, City Insight
(Pty) Ltd
South Africa

Willy Govender
Owner,
Dataworld (Pty) Ltd
South Africa

Introduction

The effectiveness of programmes realizing urban equity and resilience in the South African context are greatly constrained by South Africa's entrenched racial, (and through that class) land ownership and settlement patterns. Given the costs of well-located urban land, the state efforts to house the urban poor have often resulted in housing opportunities being provided at great distance from the urban core and employment opportunities. This has exacerbated the ability of even the working poor to make ends meet as high transport costs often consume over 25% of their income. The black working poor often have to have three homes to survive: a home where apartheid's forced removals forced them to live, a home which they may have received as a results of the democratic state's massive housing provision since 1994, and also a home in the form of a shack which is located close to their workplace and in which they live in order to reduce travel costs whilst working or seeking work.

This report analyses the spatial and economic inequities between, and within, South Africa's major metropolitan areas. It aims to better understand the spatial interlinkages between racial segregation, poverty, household composition, land value and income inequality in these areas. It examines the market valuation of property across 11 municipalities drawing out the implications of these trends for reducing inequality. These data also have implications for providing housing on well located vacant land, as well as for transforming the apartheid spatial landscape. Overall, the report will emphasise the challenges in overcoming inequality and providing access to urban opportunities for particularly poor and black South Africans who were historically disenfranchised.

National municipal context

South Africa is divided into 257 municipalities, organised into two basic groups:
- 8 Category A municipalities often referred to as Metropolitan municipalities; and
- 205 Category B municipalities (referred to as locals) which are distributed across 44 Category C municipalities (referred to as Districts).

Municipalities exercise a range of powers and functions, and in general are the major distributors of basic network services such as electricity, water, sanitation, roads, transport; as well as a number of community-based and economic services such as planning and development, parks, recreation, cemeteries and crematoria, tourism, and local economic development.

Municipalities receive a share of the national fiscus (known as the equitable share), as well as contributions from national/provincial governments to deliver a certain quantum of free basic services (water, electricity, sanitation) as well as to undertake a range of developmental functions such as providing access to electricity, water and sanitation for particularly the poor, the building of roads and the provision of public transport.

Municipalities that deliver services such as electricity, water and

sanitation are able to recover these costs through charging tariffs.

Metro and Local municipalities are also able to tax property owners through charging property rates. These taxes are calculated using a formula (termed 'rates randage') which is a proportion of the market valuation of a property, and which must be paid directly to a municipality.

The financial resources available to municipalities differs markedly across the country, with the Metros having significantly larger budgets than the Locals. The Metros have an aggregate budget of R237 ZAR Billion, compared to the rest of the municipalities have total budgets of only some R143 ZAR Billion.

The following figures indicates the significant spatial differences in municipal budgets across the country, the first map on the left showing the total municipal revenue per municipality. When the revenue data is standardised by the population size being served, the spatial inequalities become more clear, with the larger urban areas having greater resources with which to provide services to their communities. The effects of apartheid are clear in that the areas shown as blue (ie with less revenue) are largely former homeland areas. The map figure 1 indicates the extent of area of South Africa which fell under the former apartheid homeland system:

There are also significant spatial disparities when one compares municipalities in terms of the rates revenue being generated per person in each municipality. This is indicated in the map figure 2

Overall, then, there are clear spatial inequities in the funds available to municipalities to provide basic services to their communities, as well as in the funds the municipalities

are able to generate. These spatial inequities are largely a result of the legacy of apartheid, where formerly white areas had higher levels of education, higher levels of services in households (water, electricity, etc.) and higher GDP (and its effect of having higher employment levels). Hence it is no real surprise to find that there are very high levels of correlations between the billed rates and these variables which epitomised what white people under apartheid received.

On the other hand, since South Africa's democracy in 1994 in particular, significant additional numbers of black South Africans have moved to these areas of economic opportunity. In many cases these migrants move as individuals, at least initially, and seek out the least expensive forms of accommodation. There is therefore a strong correlation between the size of the property rates bill and the number of households living in backyard shacks and informal settlements. Indeed, the numbers of people living in poverty are even greater in the large urban areas.

The spatial inequities in the property rates income for municipalities is further evidenced in a review of the municipal property valuation rolls. As may be seen in the table below, 50% of properties that can be valued in terms of their market value, and which are used to generate property rates income, are
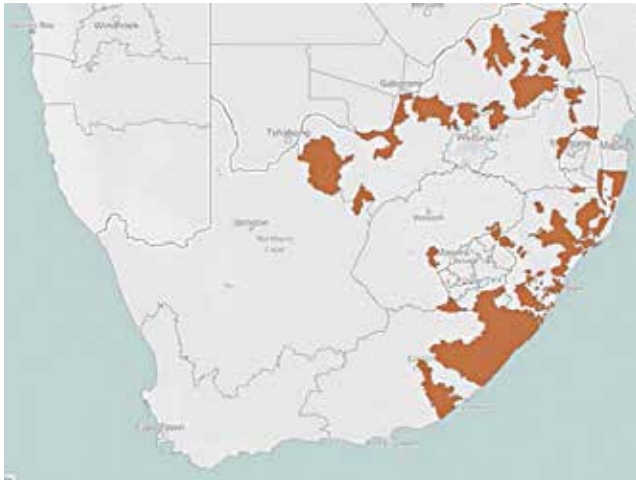
Figure 1: Former homeland areas under the apartheid system
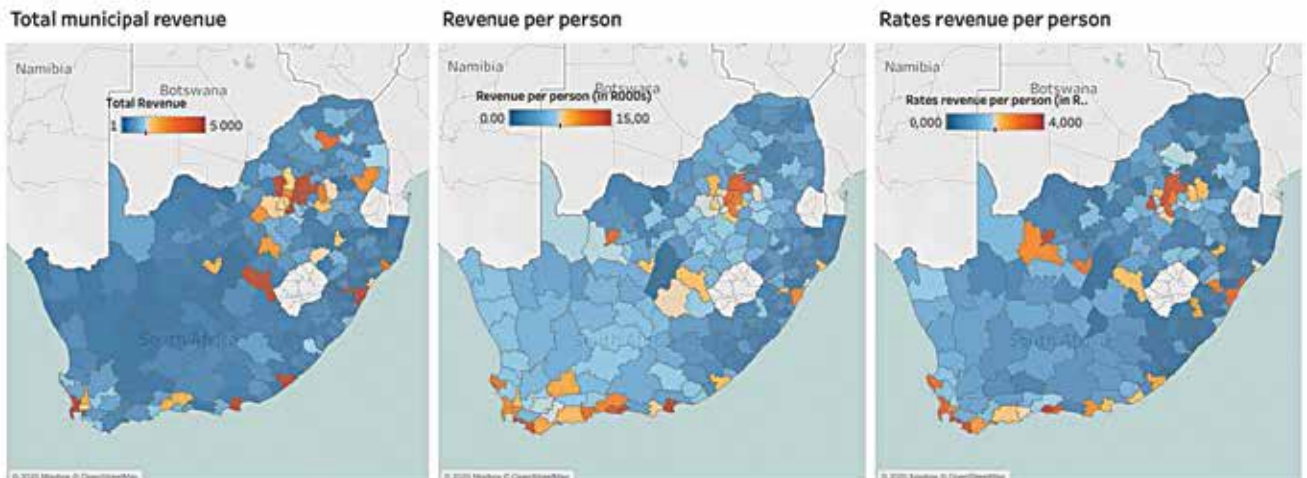
Figure 2: Total Revenue, Revenue per person and Rates Revenue per person

found in the 8 Metros which contain only around 30% of the population.

The next section looks at how, within municipalities, similar inequities exist.

The spatial distribution of market value of property within municipalities

Whilst spatial inequities with the South African municipal system are often discussed in general, and have usually focussed on the impacts that racial segregation continues to have on development progress, very few studies have provided empirical evidence showing how the inequities in access to decent housing have impacted on property markets and in turn how those markets have led to spatial inequities in property markets within municipalities.

This forms the subject of this study and in order to analyse the degree to which such inequities exist, a set of case study municipalities were chosen and databases for each developed. Eleven municipalities were selected across the larger municipalities:
• Category A: Johannesburg, Ekurhuleni, eThekwini and Nelson Mandela Bay;
• B1 - (Larger secondary city

centres): Msunduzi, Newcastle, uMhlathuze and Madibeng;
• B2 - (Regional/tertiary centres): Merafong, Ray Nkonyeni and KwaDukuza.

A brief descriptions of these municipalities follows[1]:
• **City of Johannesburg** is one of the most commercial cities in Africa and the engine room of the South African and regional economy. Johannesburg is home to almost five million people, accounting for about 36% of the Gauteng's provincial population and 8% of the national population. The city's main economic sectors are finance and business services, community services, manufacturing, trade (collectively 82%)
• **uMhlathuze**: The City of uMhlathuze Local Municipality is a Category B municipality situated within the King Cetshwayo District on the north-east coast of the KwaZulu-Natal province. It is the largest among the five municipalities that make up the district. It boasts the deepest water port, in Richards Bay, and is home to the Richards Bay Industrial Development Zone (RBIDZ), which drives the inwards investment of the City through foreign direct investments. Its main economic sectors

are: manufacturing (45.9%), mining and quarrying (11.6%), financial, real estate and business (10.7%), community, social and personal services (10.4%), transport and communication (9.1%), trade (6.3%), agriculture, forestry and fishing (3.2%)
• **City of Ekurhuleni**: The City of Ekurhuleni Metropolitan Municipality is a Category A municipality in the Gauteng province and in many ways serves as the transportation hub of the country. Its main economic sectors include manufacturing (23%), finance and business services (21.3%), community services (20%), trade (15%), transport (11%), construction (4.1%), electricity (2.3%), mining (2.3%)
• **eThekwini** is a Category A municipality in the province of KwaZulu-Natal. eThekwini is the third-largest city in the country. Its main economic sectors include: finance (22%), manufacturing (22%), community services (18%), trade (16%), transport (16%), construction (3%), electricity (2%)
• **KwaDukuza** is a Category B municipality located within the iLembe District in the KwaZulu-Natal Province. Its main economic sectors include: agriculture and tourism
• **Madibeng** is a Category B municipality located in the North West Province within the Bojanala Platinum District. Its main economic sectors include mining, manufacturing, agriculture and tourism
• **Merafong** is a Category B municipality situated within the West Rand District in the Gauteng Province. Its main economic sectors include mining (50.7%), trade (9.7%), finance and business services (9.9%), community services (9.2%), general government (9.1%)
• **Msunduzi** is a Category B municipality situated within the uMgungundlovu District in KwaZulu-Natal. Its main economic sectors include community services (29%), finance (24%), transport (13%), trade (12%), manufacturing (12%)
• **Nelson Mandela Bay** is a Category

Figure 3: Location and MIIF Category of Case Study Municipalities

A municipality and is the economic powerhouse of the Eastern Cape Province. Its main economic sectors include Manufacturing (25%), community services (23%), finance (23%), trade (13%), transport (13%)

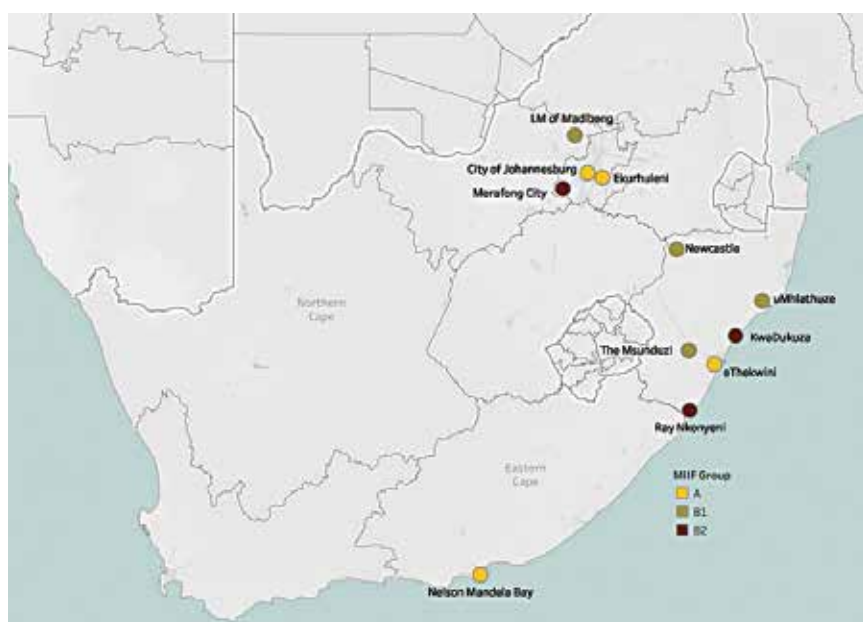- **Newcastle** is a Category B municipality situated within the Amajuba District in KwaZulu-Natal. Its main economic sectors include: Trade (24.9%), community services (22.1%), finance (14.71%), manufacturing (13.7%), construction (6.9%), transport (6.7%), agriculture (3.8%)

- **Ray Nkonyeni** is a Category B municipality situated within the Ugu District in the KwaZulu-Natal Province. Its main economic sectors include: Finance and business services (21.5%), wholesale and retail (18.7%), general government services (13.3%), manufacturing (12.3%), agriculture and forestry (8.9%), transport and communication (8.9%).

All of the case study municipalities have recently updated their general valuation rolls and they contain market valuations of at least 2,8 million properties. Collectively, these properties have been valued at around R2,8 ZAR trillion. Johannesburg itself has properties valued at over ZAR1,3 trillion whilst the smallest valuation roll of Merafongs properties are worth around ZAR19 billion.

In analysing the breakdown of properties across each of the valuation rolls by property type, the number and value of properties, we find significant variation across each of the municipalities in terms of reliance on different property sectors for their property rates income. For example, the largest *number* of properties are residential across all municipalities, but there is significant variation in the *value* of property across municipalities. For example, 88% of properties on the Johannesburg roll are residential, constituting 65% of the value of all properties. At the other end of the spectrum, in uMhlathuze whilst residential properties constitute 83% of their properties, in terms of value these are only 49% of total property value.

Business and commercial properties constitute significantly higher proportions of value than the number of properties suggest should be the case.

For purposes of analysing the spatial distribution of properties and values across each municipality, the overall number and values of all properties, as well as the specific distribution and values of residential and commercial properties are described. Three sets of analysis are provided. The first examines the degree of concentration of property values across the municipalities, the second describes the spatial distribution of property values and the third section analyses these distributions.

In examining the degree of concentration of values in specific parts of the municipality, Lorenz curves were produced, indicating:
- The cumulative proportion of property values from the smallest values to the highest property values in each ward.
- residential property values within each municipality. For these, curves were smoother indicating less concentration of residential values in wards.
- The cumulative proportion of commercial/industrial property values found across the wards and, as may be expected, they generally suggest a greater degree of concentration of commercial/industrial property values across the wards.

Overall, in order to easily compare these Lorenz curves, an adaptation of Hoover's index of concentration or localization, as cited in Cox (2019)[2], was used for comparative purposes. The indices provided in the table below are percentages which reflect the proportion of all properties that would have to be moved around in order to get equality in values (total, residential or business) in order to get complete equality across all wards in each municipality. For example, in the case of Johannesburg, in order to get equity across all wards in terms of total property values, 50% of the residential properties would have to be shifted and 60% of commercial/Industrial properties would have to be shifted. On the one hand, the results are expected in that one does not expect to find high proportions of commercial/industrial properties in all wards. But on the other hand, these concentration indices are very high lying generally close to or above 50% across all indicators and municipalities:

Clearly these data and indicators suggest that within municipalities there is a very high level of concentration of property values with some wards having high values and others very low values. This is easily evidenced in grouping the overall property values by wards across municipalities. The following table shows this, and it shows that 2 wards have overall property values of over ZAR50 Billion, with 34 wards having total property values of less than ZARR10 Million:

Table 1: Municipal case studies of valuation rolls, including dates of General valuations, number of properties in each roll and overall valuation (in Rands Million)

Code	Municipality	Property Count	Overall value (Rand Millions)
JHB	City of Joburg	914933	1303881
ETH	Ethekwini	533421	526606
EKU	City of Ekurhuleni	714226	489902
NMA	Nelson Mandela Bay	266849	134145
KZN225	City of Msunduzi	86302	83623
KZN292	KwaDukuza	45698	55299
NW372	Madibeng	62995	49593
KZN216	Ray Nkonyeni	48064	39363
KZN282	City of uMhlathuze	35605	36784
KZN252	Newcastle	58251	27966
GT484	Merafong	36153	19030

Whilst there are very high degrees of concentration of property values across the eleven case studies, it is important too to understand the spatial distribution of these property values. In order to do this Location Quotients (LQs) were calculated for each ward: high LQs indicate that the overall values are very high compared with an equitable situation. The following sets of maps for some of the municipalities reflect the spatial distribution of properties:

• Map of LQs of residential property values across all wards: these generally show that whilst the previous analysis showed there were generally high levels of concentration of property values, this map shows that the concentration of high values are generally in former white areas and the low LQs are in formerly black African areas;

• Map of LQs of commercial/business which show even higher levels of concentration but which also mirror that of the LQs of total property values;

These maps reinforce the arguments made that the spatial inequities that have their roots in apartheid continue to play a major role in the shape and form of South African cities, showing that the spatial distribution of property values and corresponds largely to the shape of the apartheid reality, with high levels of concentration (high property values in formerly white areas and low property values in formerly black areas) and spatial inequality.

A set of correlations were also calculated to show the degree to which the property values in each municipality, as dependent variables, were associated with a set of independent variables reflecting dimensions such as race, education, employment, income, housing type and access to services.

The correlation coefficients further reinforce the arguments that the racially-based apartheid system remains etched into the concrete of the country, where areas where there is a higher concentration of whites who, because of apartheid were better educated and have higher income and employment levels have high correlations with property values. Variables such as the proportion of formal housing have lower levels of correlation with property values, in part due to the fact that post-1994 the massive house building strategy of the democratic government has focussed on providing access to housing for as many, particularly poor and black, people as possible and so the sheer number of formal houses is not as good a predictor of high property values as, for example, race (white) and educational levels. At the same time, property values are inversely correlated with the proportion of black people residing in a ward:

As would be expected, a very similar situation shows when examining the correlations between residential property values and the same set of independent variables.

However, in the case of the

Table 2: Concentration indices for property values across wards in sample municipalities: total values, residential values and commercial/industrial

Name	Concentration index for residential property values	Concentration index for business/industrial property values
City of Joburg	50	60
Ethekwini	45	62
City of Ekurhuleni	43	63
Nelson Mandela Bay	41	61
Merafong	53	54
Ray Nkonyeni	61	72
City of Msunduzi	46	67
Newcastle	43	76
City of uMhlathuze	58	79
KwaDukuza	65	72
Madibeng	67	60

Table 3: Total property values across all wards broken into value bands

	JHB	ETH	EKU	NMA	KZN216	KZN225	KZN252	KZN282	KZN292	NW372	GT484	Grand Total
>R50Bn	1	1										2
R20-50Bn	21		3									24
R10-20Bn	22	14	14	1		1		1	2	1		56
R5-R10Bn	12	21	15	8	1	5		1	1			64
R2,5-R5Bn	25	13	12	8	6	6	4	3	1	4		82
R1-R2,5Bn	46	28	46	14	4	8	3	5	6	7	9	176
R500Mn-R1Bn	7	19	18	14	3	4	7	5	2	3	5	87
R250Mn-R500Mn	1	6	3	11	4	3	11	3	4	3	2	51
R100Mn-R250Mn		5	1	4	4	3	5	5	8	11	6	52
R50Mn-R100Mn		1			2	1		1	4	2	4	15
R25Mn-R50Mn		1			2	5	2	1	1	1	2	15
R1-R10Mn		1			10	3	2	2		4		22
R0-									8	4		12
Grand Total	135	110	112	60	36	39	34	34	29	41	28	658

Most municipalities do not currently charge property rates in former black townships. This is a response to high levels of poverty in these areas as well as to the fact that many townships do not have freehold tenure as they are located on traditional land. However this also allows for a situation where new housing is developed in these areas specifically because the owners do not have to pay for property rates
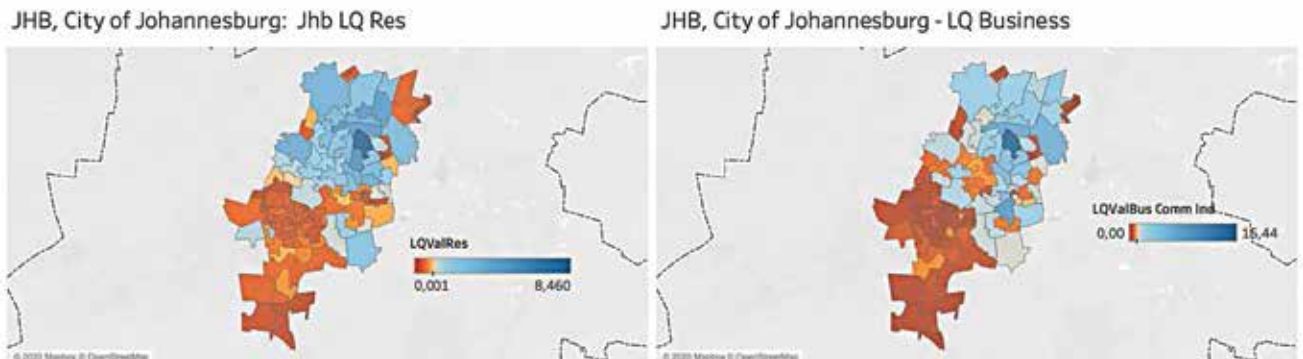

Figure 4: Spatial analysis of Property values across wards in Johannesburg

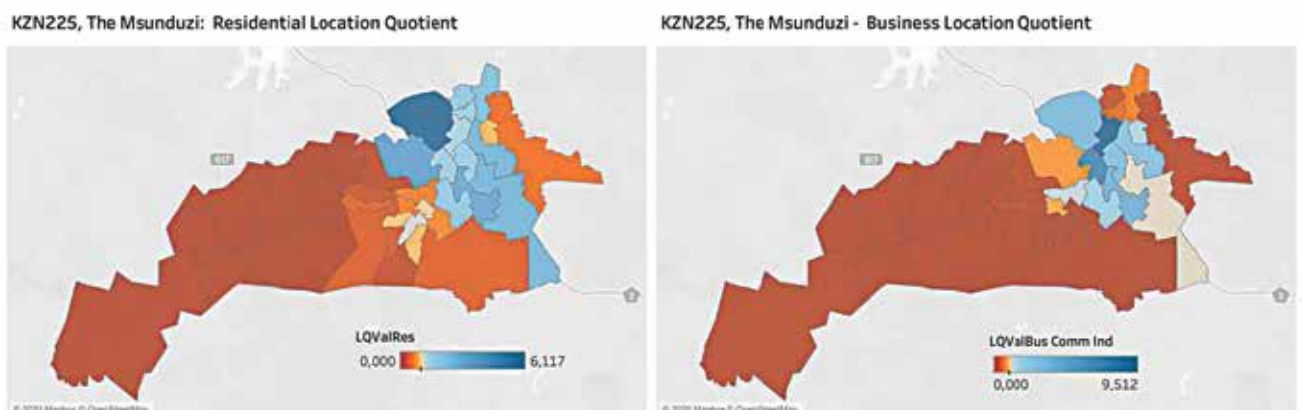**Figure 5: Spatial analysis of Property values across wards in eThekwini**

Figure 6: Spatial analysis of Property values across wards in Msunduzi

relationship between business/ commercial/industrial property values and the set of independent variables, the results are not as strong. Whilst the results still reflect the effects of apartheid, with black areas unlikely to have high business property values as compared with white areas, the reality is also that black South Africans often created and moved into informal settlements close to places of economic opportunity in the post-1994 period. As a result the strong relationships evidenced in the previous two tables, would have been diluted to a certain extent, even though the effects of the racist past are still evident.

Table 4: Correlation coefficients using Total Property Values as the dependent variable correlated with independent variables

Property Values	Johannesburg	Ekurhuleni	eThekwini	Nelson Mandela Bay	The Msunduzi	KwaDukuza	Madibeng	Ray Nkonyeni	uMhlathuze	Newcastle	Merafong City
Black	-0,47	-0,62	-0,51	-0,51	-0,66	-0,53	-0,09	-0,62	-0,42	-0,53	-0,52
White	0,75	0,82	0,68	0,81	0,76	0,90	0,80	0,87	0,83	0,78	0,73
No schooling	-0,42	-0,44	-0,38	-0,45	-0,62	-0,30	0,33	-0,55	-0,37	-0,50	-0,21
Higher Education	0,86	0,88	0,79	0,87	0,87	0,73	0,83	0,74	0,65	0,77	0,66
Unemployed	-0,61	-0,66	-0,58	-0,63	-0,64	-0,48	-0,20	-0,39	-0,38	-0,44	-0,66
Formal house	0,58	0,59	0,53	0,56	0,67	0,15	0,55	0,57	0,53	0,30	0,42
Backyard Informal	-0,24	-0,35	-0,09	-0,27	0,07	-0,23	0,15	0,22	-0,03	0,03	-0,33
No Income	-0,32	-0,39	-0,11	-0,16	-0,14	-0,32	0,15	0,01	-0,11	-0,26	-0,38
HH Income total	0,90	0,91	0,85	0,87	0,86	0,88	0,90	0,84	0,77	0,83	0,73
No energy	-0,07	-0,24	0,00	-0,22	-0,01	-0,03	0,55	-0,03	-0,26	-0,02	-0,31
No Water in house	-0,36	-0,45	-0,36	-0,53	-0,70	-0,37	0,12	-0,48	-0,51	-0,43	-0,10
No Sanitation in house	-0,12	-0,20	-0,29	-0,15	-0,69	-0,34	0,11	-0,29	-0,49	-0,38	-0,26

Table 5: Correlation coefficients using Residential Property Values as the dependent variable correlated with independent variables

Property Values	Johannesburg	Ekurhuleni	eThekwini	Nelson Mandela Bay	The Msunduzi	KwaDukuza	Madibeng	Ray Nkonyeni	uMhlathuze	Newcastle	Merafong City
Black	-0,51	-0,63	-0,53	-0,58	-0,65	-0,53	-0,13	-0,59	-0,38	-0,66	-0,58
White	0,81	0,79	0,75	0,89	0,86	0,92	0,76	0,90	0,83	0,93	0,93
No schooling	-0,44	-0,46	-0,36	-0,53	-0,58	-0,32	0,19	-0,51	-0,41	-0,64	-0,33
Higher Education	0,89	0,90	0,79	0,96	0,93	0,73	0,86	0,74	0,77	0,92	0,93
Unemployed	-0,64	-0,68	-0,58	-0,70	-0,63	-0,48	-0,18	-0,36	-0,40	-0,58	-0,41
Formal house	0,56	0,53	0,52	0,60	0,69	0,14	0,45	0,59	0,65	0,31	0,37
Backyard Informal	-0,26	-0,38	-0,10	-0,37	0,04	-0,25	0,11	0,13	0,04	-0,21	-0,32
No Income	-0,37	-0,43	-0,17	-0,23	-0,15	-0,32	0,12	-0,02	-0,08	-0,37	-0,09
HH Income total	0,94	0,94	0,90	0,98	0,97	0,88	0,89	0,83	0,87	0,97	0,83
No energy	-0,08	-0,25	-0,04	-0,30	0,06	-0,05	0,44	-0,12	-0,24	-0,31	-0,31
No Water in house	-0,38	-0,47	-0,37	-0,63	-0,69	-0,38	0,03	-0,49	-0,59	-0,58	-0,27
No Sanitation in house	-0,14	-0,23	-0,28	-0,27	-0,63	-0,34	0,02	-0,27	-0,57	-0,51	-0,28

Policy implications

The policy challenge at a national level is to create greater equity between municipalities, providing greater resources to municipalities who are faced with high levels of need, but low financial resources to address them. This needs to be done without compromising the growth of the large metro areas which accommodate growing numbers of poor migrants in search of work opportunities.

Within municipalities there is a need to:
- Increase the revenue base of municipalities, through measures which ensure that property values are able to be realised in all areas, not just former white areas. This requires mechanisms to bring 'unrated'/ traditional areas into the rates system to avoid the problem of people living and building homes in these areas to avoid property rates. This must be done whilst ensuring that poor and indigent households are not burdened with additional costs they cannot afford.
- Use increased revenue's from broadening the property rates base to improve access to services and improved urban environments for the poor and in underserved areas.
- Use the resources already available in former white areas to benefit poorer black households and allow them to get access to the city, improved social and other services and lower their costs of living.
- Develop mechanisms to use vacant land and densification as a means of improving equity whilst increasing rates

The following policy amendments are proposed

Well-located areas of opportunity

Identify well located areas within each municipality which are close

Table 6: Correlation coefficients using Business, Commercial and Industrial Values as the dependent variable correlated with independent variables

Property Values	Johannesburg	Ekurhuleni	eThekwini	Nelson Mandela Bay	The Msunduzi	KwaDukuza	Madibeng	Ray Nkonyeni	uMhlathuze	Newcastle	Merafong City
Black	-0,31	-0,38	-0,34	-0,28	-0,45	-0,50	-0,29	-0,49	-0,37	-0,20	-0,26
Coloured / Indian	0,09	0,24	0,12	0,02	0,34	0,15	0,77	0,28	0,25	0,35	0,07
White	0,52	0,56	0,39	0,37	0,36	0,69	0,70	0,44	0,72	0,26	0,17
No schooling	-0,29	-0,30	-0,30	-0,31	-0,46	-0,35	0,04	-0,43	-0,27	-0,21	-0,09
Higher Education	0,63	0,57	0,57	0,42	0,51	0,72	0,62	0,45	0,49	0,26	0,08
Unemployed	-0,44	-0,40	-0,41	-0,33	-0,42	-0,43	-0,30	-0,36	-0,29	-0,04	-0,57
Formal house	0,49	0,43	0,39	0,27	0,42	0,21	0,26	0,22	0,41	0,26	0,24
Backyard Informal	-0,17	-0,19	-0,07	-0,17	0,07	-0,18	0,16	0,39	-0,07	0,29	-0,18
No Income	-0,19	-0,19	0,02	-0,09	-0,12	-0,25	0,05	0,12	-0,08	0,07	-0,44
HH Income total	0,67	0,56	0,55	0,40	0,45	0,80	0,72	0,55	0,61	0,30	0,28
No energy	-0,08	-0,15	0,03	-0,17	-0,10	-0,09	0,41	0,15	-0,22	0,08	-0,21
No Water in house	-0,27	-0,28	-0,25	-0,30	-0,51	-0,38	-0,02	-0,32	-0,37	-0,10	0,11
No Sanitation in house	-0,13	-0,12	-0,23	-0,18	-0,54	-0,35	-0,06	-0,27	-0,36	-0,12	-0,13

Whilst South Africa's municipal system has been reformed, including the legislative system which guides it and the allocation of financial resources across municipalities, these have not addressed the spatial inequality that exists across the country as well as within cities

to job opportunities and which are in well-serviced neighbourhoods with adequate service and social infrastructure. Within each, undertake an analysis of available vacant land, as well as under-used land which can be repurposed or densified. These should be demarcated and prioritised for social or rental housing opportunities where low income households are given accommodation opportunities. These should be funded from the national fiscus (as social housing currently is).

The current housing subsidy grant – which although not discussed in this document – is a considerable quantum of funding available for housing purposes is currently used to fund and develop low income housing on inexpensive land, generally on the outskirts of urban areas, should be re-designed to focus increasingly on social housing.

Broadening municipal revenue

Most municipalities do not currently charge property rates in former black townships. This is a response to high levels of poverty in these areas as well as to the fact that many townships do not have freehold tenure as they are located on traditional land. However this also allows for a situation where new housing is developed in these areas specifically because the owners do not have to pay for property rates.

Considerable work is currently being done in looking at South Africa's tenure system and how it can be reformed to provide greater security of tenure for those living on traditional land. Whilst not the focus of this paper, it is important to recognise that there are a variety of mechanisms that could be used to levy charges on land that is communally owned. One such mechanism could be to use the sectional title or share block mechanisms.

However this must be done in a way that does not over-burden the poor, but ensures that residential structures over a certain value are taxed. The experience from the levying of tolls on highways in Gauteng "e-Tolls" must be incorporated into any initiative to levy taxes onto what has previously been free. It is important to ensure adequate consultation is held on this and initial costs are kept as low as possible.

Township focussed commercial and industrial development

In order to increase access to employment opportunities in former black townships and to address the lack of amenities in these areas, the spatial focus for industrial and commercial development should be on land within or adjacent to these areas. South Africa has experience – although with mixed degrees of success - in establishing Special Economic Zones (SEZ's) and Industrial Development Zones (IDZ's) in order to encourage development in particular spatial areas.

As above, however, it is vital to learn from the failures of some previous initiatives: development must be located in areas that are suitable for commercial development and not all outlying townships will be suitable. In addition, it is important to ensure that these do not become single land use areas, but instead are well

planned integrated zones which include business, light industry, government services as well as residential areas.

A strong infrastructure component must accompany these initiatives to ensure that former neglected areas are provided with greater access to transport, energy and water infrastructure.

Concluding comments

The above data and maps show that the spatial effects of apartheid spatial planning are still deeply etched in the national and urban landscape.

Whilst South Africa's municipal system has been reformed, including the legislative system which guides it and the allocation of financial resources across municipalities, these have not addressed the spatial inequality that exists across the country as well as within cities.

The financial system attempts to equitably allocate resources across municipalities according to their needs. Many municipalities raise revenue from the sale of services, but this does not generate significant net revenue for the municipality. Municipal income from property rates, however, can generate a far higher proportion of net profit. However, because the ability of municipalities to raise their own revenues is linked to the commercial value of property, areas that benefited from the allocation of resources under apartheid remain privileged and these benefits are being further endorsed with greater access to resources, perpetuating the apartheid legacy.

The policy proposals made aim to ensure that apartheid spatial patterns are effectively disrupted through firstly, creating space within former white residential areas for lower income black residents who will be able to benefit from the resources and facilities that were developed for whites during apartheid.

Secondly, it is proposed that there is a focussed initiative to develop infrastructure and facilities on land within or near former black townships which are located in outlying areas. These are aimed at ensuring that these former 'dormitory townships' are made into viable, liveable environments which support a greater range of land uses.

Finally, policy proposals are made to ensure that municipal own-revenue sources are increased through bringing in currently un-taxed land on which development is currently taking place.

Endnotes

[1]   See www.municipalities. co.za for municipal profiles.

[2]   Uneven Varieties of Space Economy Paper prepared for the annual conference of the Cambridge Journal of Regions, Economy and Society, July, 2019: 'Rethinking the Economy of Place: Challenges of Inclusion, Productivity and Power.'

Finding other earths by surveying space dust

A team of scientists found NASA's Nancy Grace Roman Space Telescope will be able to measure a specific kind of space dust littered throughout dozens of nearby planetary systems' habitable zones, or the regions around stars where temperatures are mild enough that liquid water could pool on worlds' surfaces. Finding out how much of this material these systems contain would help astronomers learn more about how rocky planets form and guide the search for habitable worlds by future missions.

In our own solar system, zodiacal dust – small rocky grains largely left behind by colliding asteroids and crumbling comets – spans from near the Sun to the asteroid belt between Mars and Jupiter. Seen from a distance, it's the brightest thing in the solar system after the Sun. In other planetary systems it's called exozodiacal dust and creates a haze that obscures our view of planets because it scatters light from the host star.

By studying exozodiacal dust, astronomers can find clues to what other planetary systems are like. The amount of debris hints at comet activity, since a greater number of comets should produce more dust. Seeing the dust's distribution pattern could offer hints about orbiting planets, which could sculpt the debris with their gravity and carve paths through the material.

While other observatories, such as the Hubble Space Telescope, have observed cold debris disks far from their host stars – farther from their stars than Neptune is from the Sun – no one has been able to photograph warm dust in the habitable zone region. While previous NASA projects have made preliminary measurements of exozodiacal dust in habitable zones, Roman's images will be much more sensitive, thanks to its advanced high-contrast Coronagraph Instrument and its stable location in space. Orbiting a million miles from Earth around the Lagrange Point 2 (L2), instead of in low-Earth orbit like Hubble, means our planet won't present such a challenging environment from which to make these observations.

Imaging warm debris closer to host stars is important because it's made up of different material than outer dust disks. Closer to the host star, rocky grains dominate the dust; farther away, it is largely composed of icy grains. The debris in each region is created by different processes, so studying the chemistry of exozodiacal dust offers information astronomers can't get by observing the outer regions around other stars.

By Ashley Balzer
NASA's Goddard Space Flight Center, Greenbelt, Md.

www.nasa.gov

Mapping the urban atmospheric carbon stock

We present this study in two parts. In this part, the materials and methods are discussed. The results of the study will be published in May 2022 issue of Coordinates

MD Abdul Mueed Choudhury

Department of Agricultural, Food, and Environmental Sciences, Marche Polytechnic University, 60131 Ancona, Italy

Ernesto Marcheggiani

Department of Agricultural, Food, and Environmental Sciences, Marche Polytechnic University, 60131 Ancona, Italy
Division of Forest, Nature, and Landscape, Department of Earth and Environmental Sciences, KU Leuven, 3001 Leuven, Belgium

Andrea Galli

Department of Agricultural, Food, and Environmental Sciences, Marche Polytechnic University, 60131 Ancona, Italy

Giuseppe Modica

Dipartimento di Agraria, Università degli Studi Mediterranea di Reggio Calabria, Località Feodi Vito, 89122 Reggio Calabria, Italy

Ben Somers

Division of Forest, Nature, and Landscape, Department of Earth and Environmental Sciences, KU Leuven, 3001 Leuven, Belgium

Abstract

Currently, the worsening impacts of urbanizations have been impelled to the importance of monitoring and management of existing urban trees, securing sustainable use of the available green spaces. Urban tree species identification and evaluation of their roles in atmospheric Carbon Stock (CS) are still among the prime concerns for city planners regarding initiating a convenient and easily adaptive urban green planning and management system. A detailed methodology on the urban tree carbon stock calibration and mapping was conducted in the urban area of Brussels, Belgium. A comparative analysis of the mapping outcomes was assessed to define the convenience and efficiency of two different remote sensing data sources, Light Detection and Ranging (LiDAR) and WorldView-3 (WV-3), in a unique urban area.

The mapping results were validated against field estimated carbon stocks. At the initial stage, dominant tree species were identified and classified using the high-resolution WorldView3 image, leading to the final carbon stock mapping based on the dominant species. An object-based image analysis approach was employed to attain an overall accuracy (OA) of 71% during the classification of the dominant species. The field estimations of carbon stock for each plot were done utilizing an allometric model based on the field tree dendrometric data. Later based on the correlation among the field data and the variables (i.e., Normalized Difference Vegetation Index, NDVI and Crown Height Model, CHM) extracted from the available remote sensing data, the carbon stock mapping and validation had been done in a GIS environment. The calibrated NDVI and CHM had been used to compute possible carbon stock in either case of the WV-3 image and LiDAR data, respectively. A comparative discussion has been introduced to bring out the issues, especially for the developing countries, where WV-3 data could be a better solution over the hardly available LiDAR data. This study could assist city planners in understanding and deciding the applicability of remote sensing data sources based on their availability and the level of expediency, ensuring a sustainable urban green management system.

1. Introduction

To date, rapid urbanization intensely poses the need for greener landscapes in many urban areas worldwide. Green spaces allow maximizing urban resilience and livability and to positively respond to climate change effects. While cities are striving for more green space, more than half of the earth's population is already living in cities, and by 2050, 66% will be city dwellers [1]. Overexploitation of environmental resources for the huge population is indeed increasing the vulnerability of the urban dwellers to natural hazards.

To keep pace with rapid urbanization, efficient urban green planning could be nothing but a time being and an expeditious solution. Conservation and expansion of existing urban vegetation based on their structural and functional roles in an urban atmosphere are some of the most effective factors of green urban

planning. Thus, various approaches based on advanced technologies have been implemented to assess the contributions of urban trees, especially evaluation of their roles in atmospheric Carbon Stock (CS) is being increasingly acknowledged [2,3]. Trees in city streets and parks are now being recognized as a key tool against impacts caused by the increased rate of atmospheric carbon dioxide (CO_2) concentrations [4–7], since they sequester atmospheric carbon during the whole growth process and at the same time delay the adverse effects of climate change contributing to the accumulation of carbon in the soil [8–10]. Studies found that the total yearly reduction in carbon emission can be up to 18 kg/tree in urban areas [11–13], which clearly brings out the importance of planting trees along with having an efficient tree management policy, especially in a complex city environment. Trees directly impact atmospheric CO_2 fixation through photosynthesis, but in urban areas, the process is quite fitful due to tree health issues. As it is well known that the well-grown trees store far more carbon than the poorly grown ones, in urban areas, it is a huge challenge to maintain and preserve mature trees and well-managed urban forests that also include tree plantations and replacements. Therefore an efficient and timewise monitoring approach is essential to introduce an adequate urban tree management system [14,15]. In addition an effective monitoring system could be ensured utilizing an accurate and convenient species-based CS mapping approach. Most of the CS calibration and predictive models are based on the estimation of Above Ground Biomass (AGB) production [13,16–20], which is considered to be primarily responsible for the atmospheric CS [10,21–23]. In this study, the AGB was estimated based on the tree allometric information (i.e., Height (H), Diameter at Breast Height (DBH)) collected during the field surveys.

Currently, remote sensing-based mapping has been availed as an influential approach in monitoring functional and structural urban tree features to policymakers [24–31]. In fact, spatially extracted information on tree species and habitats over large areas are significant in understanding species' roles, such as in providing ecosystem functions and services [32–35]. Over the last few decades, remote sensing-based classification of tree species has been widely utilized either in the case of mapping specific species-based ecosystem services (ES) outcomes (i.e., [36]), or growth and yield models and, etc. (e.g., [33,37,38]). Remote sensing approaches, especially hyperspectral imagery, have significantly upgraded the tree classification outcomes either in single trees or mixed populations [33,39–43]. The utilization of very high spatial resolution multispectral satellite imagery (e.g., 1-m IKONOS, 0.6-m QuickBird) and aerial photos/digital imagery has been rapidly increased, especially in spatial mapping [44–47]. As a matter of fact, recently, with the advancements of remote sensing technologies, a diversified type of very high resolution remotely sensed images (such as WorldView-3, WV-3) are commercially available, certainly introducing a wave of opportunities for the accurate mapping of urban trees at a significant level [31,33,48–52]. Moreover, in the case of this study, a high-resolution WV-3 image has been successfully utilized to classify the dominant tree species in Brussels, which has been found useful for further CS mapping as it was earlier in the case of Sassuolo [36].

Additionally, there are also many convincing applications of Light Detection and Ranging (LiDAR) based calibration of the tree CS utilizing the individual tree metrics (i.e., [53–61]). On the other hand, much less evidence is available in the CS calibration of the urban trees utilizing only the multispectral satellite data [11]. In the case of urban areas, tree species mapping is still a considerable challenge due to having spatially heterogeneous land cover types from isolated trees to the dense forest, high tree species diversity along with heavily and regularly managed trees, as well as the interruptions by buildings and their shadows [7,62–66]. Considering these facts, Geospatial Object-Based Image Analysis (GEOBIA) has been utilized in this study to classify the dominant tree species.

However, it is yet a crucial concern to dig out the most convenient and compatible ways to map and predict the urban tree CS in a specific urban area. A method could be considered convenient in various ways, such as its application, time consumption, and execution expenses. Even LiDAR application is the most acceptable and widely reliable, it is still expensive and hardly cost-effective for the more significant part of the world. Therefore, it would be a timely consideration to analyse the utilization of multispectral satellite data (i.e., Sentinel-2, WorldView-2/3/4) regarding CS computation possibilities of the trees in an urban area. A remote sensing-based biomass assessment has been employed in many studies [10,67–69] to obtain forest information over a large area at a reasonable cost with acceptable accuracy and minimal effort [70]. It is also evident that the method of determining relationships between field estimations and remote sensing data-derived variables and then extrapolating these relationships over large areas is very useful [10,71–78]. Here, the main goal of this study was to map the urban tree CS based on field measurements and the application of remote sensing tools considering the following:

• A comparative analysis of the application of two different remote sensing data sources (i.e., LiDAR and WV-3 image data) regarding CS mapping in the case of dominant urban tree species;
• To recommend an approach in the case of CS mapping for policymakers involving urban green management.

In a word, this study has been done to provide a fundamental tool considering urban CS mapping, which is one of the most critical issues for sustainable urban green management systems and their policymakers.

Figure 1. The study area at the eastern part of the urban area in Brussels (Belgium)

Figure 2. The map shows the distribution of sample and validation point to the estimation of Carbon Stocks (CS) superimposed over the WorldView–3 (WV–3) image data of the study area in Brussels.

2. Materials and Methods

2.1. Dataset

2.1.1. Field Data

The study area, covering an area of around 49 km^2 in the eastern part of the capital region in Belgium (Figure 1), was selected considering the availability of airborne LiDAR.

As the main goal of this study was to identify only the dominant urban tree species, all other non-dominant vegetations have been excluded during sampling. The sample plots were randomly selected, covering only the streets of the whole study area. Since in the parks most of the cases of tree crowns were overlapped and or completely overshadowed by the other species. That is why overcrowded tree populations were excluded to avoid misinterpretations of the species dominance information, during the final CS mapping. During field data collection, 75 plots (yellow dots in Figure 2) of 100 m^2 (10 m × 10 m) each were selected throughout the study area following the well-known Simple Random Sampling (SRS) approach [79–82]. Only the areas with tree species dominance (i.e., woody or tall perennial plants) have been considered, excluding the ornamental herbs, shrubs, or grassland areas. The sample plots were also used during the training and validation of the tree species for GEOBIA classification. Among the 75 plots, 20 plots (red square boxes in Figure 2) were considered for the CS mapping and validation. The Diameter at Breast Height (DBH) was measured for each tree in the plot. The height (H) of trees was measured utilizing the hypsometer Nikon Forestry 550, a laser rangefinder with angle compensation technology optimized for forestry use [83], and a field computer was used to mark the plots on QGIS. Field data (H, DBH) were collected in the summer of 2019.

2.1.2. Remote Sensing Data

The airborne LiDAR dataset had been collected in Summer 2015 by Aerodata
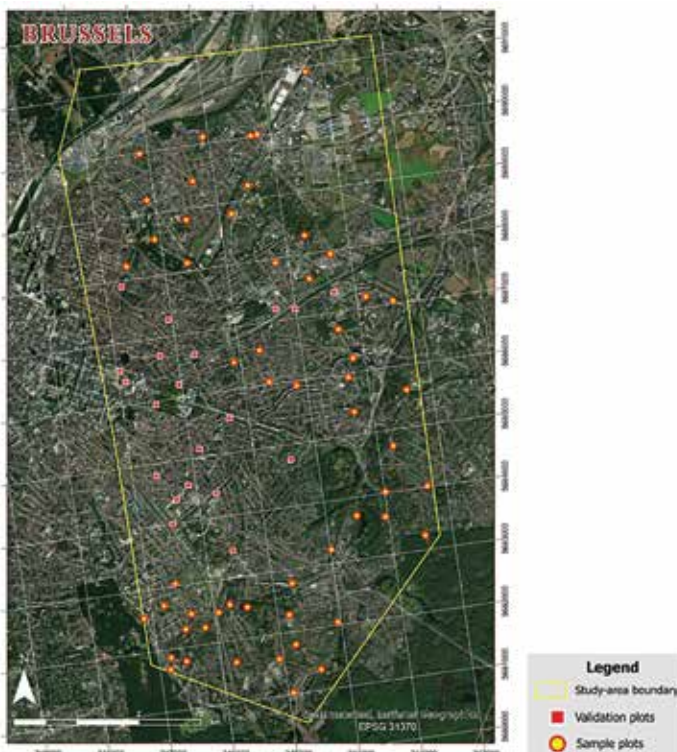
Surveys Nederland BV [84]. The Crown Height Model (CHM), i.e., the height of objects obtained through the difference between the digital surface model (DSM) and the digital terrain model (DTM), was produced at a spatial resolution of 0.25 m using the LAStools software [84].

The WV3 image data for this study was acquired on 17 April 2017 (Figure 2), which provides one panchromatic band of 0.3 m and eight multispectral bands at 1.2 m spatial resolution (Table 1). The available WV-3 image data have been pan-sharpened at the initial stage. Pan-sharpening is the process of merging high-resolution panchromatic and multispectral imagery where the outcome is an image that has the high spectral resolution tion of the multispectral image and also the high spatial resolution of the panchromatic image [85–87].

The pan-sharpen process was conducted using the hyperspectral colour sharpening (HCS) algorithm that combines the high-resolution panchromatic data with lower res-olution multispectral data and specifically implemented for the WV imagery [88]. The cubic convolution resampling technique was chosen to resample the multispectral image to the high-resolution image using a 4×4 pixel moving window. The pan image and the multispectral image have been separately orthorectified using the DSM downloaded from the GeoPunt portal [89] and the available LiDAR data. All the steps were conducted in an ERDAS Imagine environment [90]. Later, the required shapefiles (for classification in Ecognition)

were educed from the UrbIS database (UrbIS P& B and UrbIS-Adm), a general GIS database of the Brussels region [91].

2.2. Methodology

2.2.1. Geospatial Object-Based Image Analysis (GEOBIA) Classification

Tree species classification based on spectral properties is quite a matter of con-tention due to the high intra-class spectral heterogeneity and/or inter-class spectral similarities [7,44,64–66]. The traditional pixel-based procedures, which classify each object only based on a distinct spectral signature (ignoring other spatial/contextual informa-tion) [48,92,93], are hardly capable of reaching an acceptable accuracy [94,95]. In our

study, GEOBIA was applied, which is already approved as an efficient technique in the case of high-resolution image classifications [48,85,92,96–99]. Instead of the single pixels, the GEOBIA approach typically works on: (i) Segmenting a remote sensing image into spectral similarities (i.e., segments or objects), and (ii) Evaluating the spectral, spatial, and/or context features of these segments for image classification [48,63,94,100,101]. As a result of segmentation, this approach can consider the textual and contextual information along with the spectral information during the classification [48,94,102–104]. Therefore GEOBIA classification outcomes are more acceptable than those based on the existing traditional pixel-based approach [102,105–111].

Table 1. The eight multispectral bands of the WorldView-3 (WV-3) satellite imagery.

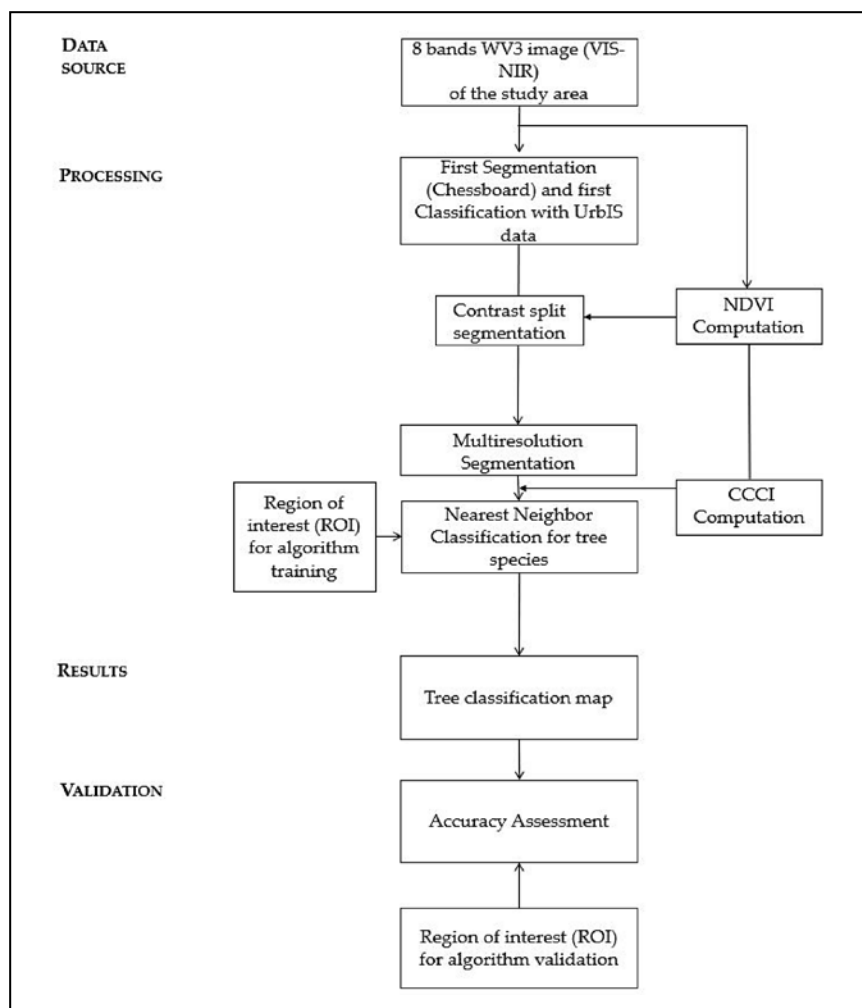| Bands	Wavelength [nm]
Coastal band	400–450
Blue band	450–510
Green band	510–580
Yellow band	585–625
Red band	630–690
Red edge band	705–715
Near-Infrared (NIR)1 band	770–895
Near-Infrared (NIR)2 band	860–1040

Figure 3. The Geospatial Object-Based Image Analysis (GEOBIA) approach of tree classification utilizing Trimble eCognition Developer® 9 platform in Brussels.

The Trimble eCognition Developer® 9 platform (Trimble, Munich, Germany) [112] was utilized to classify the dominant tree species in Brussels (Figure 3). At the initial stage, the chessboard segmentation has been introduced to initiate the GEOBIA classification approach. Then the primary classification was done utilizing the available shapefile from the Urbis database [91]. After that, the contrast split segmentation algorithm was implied to define the green and non-green areas with higher accuracy. This approach is based on the Normalized Difference Vegetation Index (NDVI) layer, where the 'contrast split' segments the scene into the dark and bright image objects based on a threshold value that maximizes the contrast between them [113]. The algorithm utilizes the optimal threshold separately for each image object which initiates a chessboard segmentation of variable scale and then performs the split on each square [114,115]. It was found quite helpful to identify the shadows, pathways, and pavements between the tree crowns.

Subsequently, the multiresolution segmentation (MRS) algorithm [116] was performed to group contiguous pixels into areas (i.e., segments) geometrically and radiometrically homogenous. The MRS algorithm was set by tuning the following parameters such as the "smoothness/compactness" that determines the preferred shape of segments, and the "colour/shape" parameter that controls the weights of spectral and shape information in the calculation of segments heterogeneity [48,94,117,118]. Considering the study of Choudhury et al. [36], green areas and streets have been identified with very large objects (as the size of the shapefile

polygons) and have been classified separately from the rest. In these areas, a subsequent multiresolution segmentation had been applied to have the smaller objects. For this segmentation, rather than the thematic layers, the spectral information and the geometric information of WV-3 bands have been considered. The segmentation was done several times utilizing a different number of values for each parameter. For scale, the values were within 5 to 30, whereas for the shape and compactness, the values were between 0.1 to 0.9 [48,94,117,118]. After several attempts with different values, the ideal values utilized for segmentation, were found as scale parameter = 10, shape = 0.5 and the compactness = 0.8.

Before starting the Nearest Neighbour (NN) approach, an index known as Canopy Content Chlorophyll Index (CCCI) is used to separate the grasses from the vegetation class. This index can be calibrated as follows,

$$CCCI = NDRE/NDVI2$$

where,

Normalized Difference Red Edge index [119]

$$NDRE = NIR2 - Red\ Edge/NIR2 + Red\ Edge,$$

$$NDVI2 = NIR2 - Red/NIR2 + Red$$

Then the Nearest Neighbour (NN) algorithm [120] was performed, which is a supervised classification technique that classified all objects in the entire image based on the selected samples and the defined statistics [94]. For the sample selection and algorithm training, the sample plots had been considered. Once the algorithm training had been done, classification was initiated utilizing the "Assign class" algorithm. Three dominant tree species have been classified, such as *Tilia* spp. L., *Acer* spp. L. and *Aesculus hippocastanum* L. [121] covering the whole study area in Brussels. In this case, the larger and intensely green parks were not considered as it was hardly possible to differentiate crowns from a mixed or overlapped tree species population. Moreover, those trees could not be considered in further CS (AGB estimation) mapping due to the larger difference between the street and the park environment concerning tree health issues. Validation of the classification outcomes (Table 2) had also been done at the Trimble eCognition Developer® 9

Table 2. Validation results expressed in percentage for the trees in Brussels.

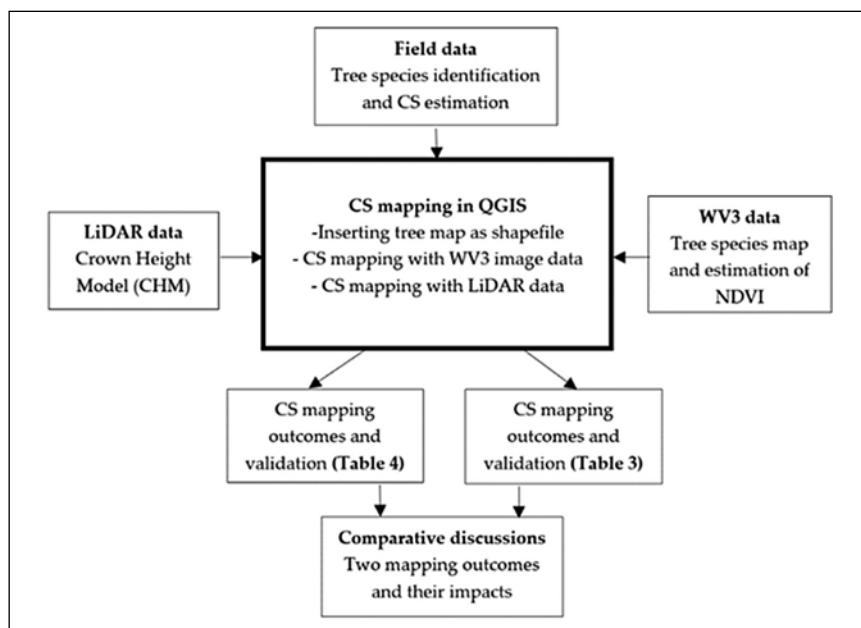|	*Acer spp.*	*Tilia spp.*	*Aesculus hippocastanum*
PA [1]	0.80	0.69	0.67
UA [1]	1	0.69	0.61
Hellden	0.89	0.69	0.64
KIA per Class	0.77	0.42	0.5
Overall Accuracy	0.71		
KIA	0.53		

[1] PA: Producer Accuracy, UA: User Accuracy.

Figure 4. The overall methodology of Carbon Stock (CS) mapping, based on the combined use of CHM and NDVI, in the urban area of Brussels.

platform [112] using confusion matrices [122–124] which is usually applied to compare the true classes with the ones assigned by the classifier on the generated maps. During the validation, 10%–15% of the total area for each class had been chosen as "true samples", as known species or classes, to train the algorithm. The estimated producer accuracy shows the completeness of classification, and the user accuracy indicates the correctness of the classes [36,125], while the Hellden parameter is used to estimate the mean accuracy for each class. The mean accuracy for each class i can be calculated using the equation presented in [36,126]:

$$\text{Mean accuracy (i)} = \frac{2A}{B+C}100\%$$

where A is the number of correctly classified reference points for class i, B is the total number of reference points in class i in the reference data, and C is the total number of reference points classified into class i.

In Table 2, KIA known as Kappa Index of Agreement (or Cohen's kappa coefficient), estimates the proportion of agreements [36,127]. Moreover, the overall accuracy (OA) has been estimated, which is the ratio of the sum of diagonal values of the confusion matrix to the total number of cell counts in the matrix [36,128].

2.2.2. Carbon Stock (CS) Mapping

Several studies suggest that tree AGB is the most visible, dominant, dynamic, and essential pool of the terrestrial ecosystem [8,129–131], constituting around 30% of the total terrestrial ecosystem carbon pool [132]. In this study, based on the relationships among the WV-3 (NDVI) data and LiDAR (CHM) data derived variables and the field data, the predictive AGB estimation and, eventually, CS mapping has been done in both cases (Figure 4).

At first, the total AGB was calculated based on the field data (i.e., DBH, H, tree species, etc.) for each of the sample plots. For this calculation, an allometric model [133] was implied to calculate

Table 3. The results obtained during the validation of estimated CS in the validation plots.

Plot ID	Tree Species	Mean CS (Field Estimation) kg/Plot	CS in QGIS Estimation (kg/Plot)	Difference (Field and QGIS)
1	Acer spp.	689.49	426.0	263.49
2	Acer spp.	930.91	397.8	533.11
3	Acer spp.	224.04	285.0	60.96
4	Aesculus hippocastanum	216.95	581.1	364.15
5	Tilia spp.	302.25	158.2	144.05
6	Acer spp.	534.17	355.5	178.67
7	Tilia spp.	277.49	411.9	134.41
8	Acer spp.	188.18	31.3	156.88
9	Acer spp.	332.73	242.8	89.93
10	Tilia spp.	626.63	341.4	285.23
11	Tilia spp.	277.97	538.8	260.83
12	Tilia spp.	64.1	214.6	150.47
13	Acer spp.	698.78	397.8	300.98
14	Aesculus hippocastanum	641.46	341.4	300.06
15	Tilia spp.	112.44	271.0	158.56
16	Acer spp.	466.16	341.4	124.76
17	Tilia spp.	97.31	45.4	51.91
18	Acer spp.	121.50	369.6	248.10
19	Aesculus hippocastanum	577.99	609.3	31.31
20	Acer spp.	316.80	200.5	116.30

Table 4. The results obtained during the estimation of CS in the validation plots.

Plot ID	Tree Species	Mean CS (Field Estimation) kg/Plot	CS in QGIS Estimation (kg/Plot)	Difference (Field and QGIS)
1	Acer spp.	689.49	761.3	71.81
2	Acer spp.	930.91	548.6	382.31
3	Acer spp.	224.04	343.5	119.46
4	Aesculus hippocastanum	216.95	188.5	28.45
5	Tilia spp.	302.25	356	53.75
6	Acer spp.	534.17	675	140.83
7	Tilia spp.	277.49	283.3	5.81
8	Acer spp.	188.18	230.9	42.72
9	Acer spp.	332.73	670.3	337.57
10	Tilia spp.	626.63	790.2	163.57
11	Tilia spp.	277.97	462.6	184.63
12	Tilia spp.	64.13	57.6	6.53
13	Acer spp.	698.78	696.9	1.88
14	Aesculus hippocastanum	641.46	179	462.46
15	Tilia spp.	112.44	200.2	87.76
16	Acer spp.	466.16	464.5	1.66
17	Tilia spp.	97.31	188.3	90.99
18	Acer spp.	121.5	93.9	27.6
19	Aesculus hippocastanum	577.99	599.4	21.41
20	Acer spp.	316.8	283.8	33

the AGB for each plot. The mean AGB/ plot estimation was necessaryas it is recommended that the tree above ground CS is assumed to be 50% of the total AGB [134–138]. Then to estimate the mean CS/plot, the mean AGB/plot was multiplied by 0.5 as a conversion factor [139–141]. Then in QGIS utilizing the WV-3 image data (from 2017, see Section 3.2.1 for details), the NDVI (Red edge and NIR1 band) of the whole study area was computed. The NDVI layer was considered in this study for the CS prediction and mapping, as previous studies claimed to find a strong correlation between the NDVI and total AGB of the trees [11,142–144]. In the case of LiDAR data, the CHM was utilized to map the CS for the dominant tree species. Then the NDVI-derived metrics were extracted for the sample plots utilizing the "Zonal statistics" plugin [145] at the QGIS interface. The CHM-derived matrices had been computed in the case of available LiDAR data (from 2015, see Section 3.2.2 for details). After that, the linear regression models were created in a Microsoft® Excel™ spreadsheet, calibrating the correlation between the mean CS/plot and the NDVI derived metrics to find out the best model to estimate and map the CS covering the whole study area [36]. The CHM-derived matrices have also been done to determine the best model concerning the perspective CS mapping. A fishnet of 100 m2 (10 10 m) resolution (as for the sample plots) was built in QGIS for both cases (NDVI and CHM) to recognize the minimum to maximum CS zones, based on the dominant species map (exported as a shapefile in QGIS) obtained from the WV-3 image data. The classification shapefile was essential to define the regions of interest, providing QGIS to map the estimated CS values considering only the dominant tree species [36]. Otherwise, the map will show the CS values for other areas, i.e., the area covered with grass or even in an area where there is no vegetation.

Then, to validate the mapping outcomes, 20 randomly selected plots have been utilized in both cases (NDVI and CHM).

This time the linear regression models were created only for the validation plots. Therefore, the differences (Tables 3 and 4) among the QGIS computed CS values, and the ground truth-values were shown to recognize the methodology's effectiveness. The validation plots were the same in both cases, which was necessary to compare the impacts and to discuss the prospects and convenience of CS mapping in urban areas (see Section 4.2 for details).

References

1. 2014 Revision of the World Urbanization Prospects|Latest Major Publications—United Nations Department of Economic and Social Affairs. Available online: https://www.un.org/en/development/desa/publications/2014-revision-world-urbanization-prospects.html (accessed on 5 May 2021).

2. Tzoulas, K.; Korpela, K.; Venn, S.; Yli-Pelkonen, V.; Ka´zmierczak, A.; Niemela, J.; James, P. Promoting ecosystem and human health in urban areas using Green Infrastructure: A literature review. *Landsc. Urban Plan*. **2007**, *81*, 167–178. [CrossRef]

3. de Vries, S.; van Dillen, S.M.; Groenewegen, P.P.; Spreeuwenberg, P. Streetscape greenery and health: Stress, social cohesion and physical activity as mediators. *Soc. Sci. Med*. **2013**, *94*, 26–33. [CrossRef] [PubMed]

4. Doick, K.J.; Davies, H.J.; Moss, J.; Coventry, R.; Handley, P.; Vazmonteiro, M.; Rogers, K.; Simpkin, P. *The Canopy Cover of England's Towns and Cities: Baselining and Setting Targets to Improve Human Health and Well-Being*; University of Birmingham: Birmingham, UK, 2017; pp. 5–6.

5. Endreny, T.; Santagata, R.; Perna, A.; De Stefano, C.; Rallo, R.; Ulgiati, S. Implementing and managing urban forests: A much needed conservation strategy to increase ecosystem services and urban wellbeing. *Ecol. Model*. **2017**, *360*, 328–335. [CrossRef]

6. Nowak, D.J. *Assessing Urban Forest Effects and Values: New York City's Urban forest (Vol. 9)*; US Department of Agriculture, Forest Service, Northern Research Station: Madison, WI, USA, 2007.

7. Baines, O.; Wilkes, P.; Disney, M. Quantifying urban forest structure with open-access remote sensing data sets. *Urban For. Urban Green*. **2020**, *50*, 126653. [CrossRef]

8. Issa, S.; Dahy, B.; Ksiksi, T.; Saleous, N. A Review of Terrestrial Carbon Assessment Methods Using Geo-Spatial Technologies with Emphasis on Arid Lands. *Remote Sens*. **2020**, *12*, 2008. [CrossRef]

9. Jo, H.-K.; Kim, J.-Y.; Park, H.-M. Carbon reduction and planning strategies for urban parks in Seoul. *Urban For. Urban Green*. **2019**, *41*, 48–54. [CrossRef]

10. Behera, S.K.; Sahu, N.; Mishra, A.K.; Bargali, S.S.; Behera, M.D.; Tuli, R. Aboveground biomass and carbon stock assessment in Indian tropical deciduous forest and relationship with stand structural attributes. *Ecol. Eng*. **2017**, *99*, 513–524. [CrossRef]

11. Kanniah, K.D.; Muhamad, N.; Kang, C.S. Remote sensing assessment of carbon storage by urban forest. *IOP Conf. Ser. Earth Environ. Sci*. **2014**, *18*, 12151. [CrossRef]

12. Rosenfeld, A.H.; Akbari, H.; Romm, J.J.; Pomerantz, M. Cool communities: Strategies for heat island mitigation and smog reduction. *Energy Build*. **1998**, *28*, 51–62. [CrossRef]

13. Ferrini, F.; Fini, A. Sustainable Management Techniques for Trees in the Urban Areas. (2011): 1–19.

14. Steenberg, J.W.; Duinker, P.N.; Nitoslawski, S.A. Ecosystem-based management revisited: Updating the concepts for urban forests. *Landsc. Urban Plan*. **2019**, *186*, 24–35. [CrossRef]

15.   Nitoslawski, S.A.; Galle, N.J.; Bosch, C.K.V.D.; Steenberg, J.W. Smarter ecosystems for smarter cities? A review of trends, technologies, and turning points for smart urban forestry. *Sustain. Cities Soc*. **2019**, *51*, 101770. [CrossRef]

16.   Brack, C.L.; James, R.N.; Banks, J.C. Data Collection and Management for Tree Assets in Urban Environments. Proceeding Urban Data Management Symposium, 1999.

17.   Brack, C. Pollution mitigation and carbon sequestration by an urban forest. *Environ. Pollut*. **2002**, *116*, S195–S200. [CrossRef]

18.   Banks, J.; Brack, C.; James, R. Modelling changes in dimensions, health status, and arboricultural implications for urban trees. *Urban Ecosyst*. **1999**, *3*, 35–43. [CrossRef]

19.   Nowak, D.J.; Crane, D.E. Carbon storage and sequestration by urban trees in the USA. *Environ. Pollut*. **2002**, *116*, 381–389.[CrossRef]

20.   Nowak, D.J. Chicago's Urban Forest Ecosystem: Results of the Chicago Urban Forest—E. Gregory McPherson—Google Books. Available online: https://books.google.it/books?hl=en&lr=&id=RnT26_xGC-4C&oi=fnd&pg=PA83&ots=G9uEFurr1T&sig=4B7P3Onwpe9Qp84zgMYDsorMViw&redir_esc=y#v=onepage&q&f=false (accessed on 9 January 2021).

21.   Mokany, K.; Raison, R.J.; Prokushkin, A. Critical analysis of root: Shoot ratios in terrestrial biomes. *Glob. Chang. Biol*. **2005**, *12*, 84–96. [CrossRef]

22.   Achard, F.; Eva, H.D.; Stibig, H.-J.; Mayaux, P.; Gallego, J.; Richards, T.; Malingreau, J.-P. Determination of Deforestation Rates of the World's Humid Tropical Forests. *Science* **2002**, *297*, 999–1002. [CrossRef] [PubMed]

23.   Brown, S. *Estimating Biomass and Biomass Change of Tropical Forests: A Primer*; Food & Agriculture Org.: Roma, Italy, 1997; Volume 134.

24.   Liu, L.; Coops, N.C.; Aven, N.W.; Pang, Y. Mapping urban tree species using integrated airborne hyperspectral and LiDAR remote sensing data. *Remote Sens. Environ*. **2017**, *200*, 170–182. [CrossRef]

25.   Dalponte, M.; Bruzzone, L.; Gianelle, D. Fusion of hyperspectral and LIDAR remote sensing data for classification of complex forest areas. *IEEE Trans. Geosci. Remote Sens*. **2008**, *46*, 1416–1427. [CrossRef]

26.   Alonzo, M.; McFadden, J.P.; Nowak, D.J.; Roberts, D.A. Mapping urban forest structure and function using hyperspectral imagery and lidar data. *Urban For. Urban Green*. **2016**, *17*, 135–147. [CrossRef]

27.   Zhang, Y.; Shen, W.; Li, M.; Lv, Y. Assessing spatio-temporal changes in forest cover and fragmentation under urban expansion in Nanjing, eastern China, from long-term Landsat observations (1987–2017). *Appl. Geogr*. **2020**, *117*, 102190. [CrossRef]

28.   Zhang, M.; Du, H.; Mao, F.; Zhou, G.; Li, X.; Dong, L.; Zheng, J.; Zhu, D.; Liu, H.; Huang, Z.; et al. Spatiotemporal Evolution of Urban Expansion Using Landsat Time Series Data and Assessment of Its Influences on Forests. *ISPRS Int. J. Geo. Inf*. **2020**, *9*, 64.[CrossRef]

29.   Shen, G.; Wang, Z.; Liu, C.; Han, Y. Mapping aboveground biomass and carbon in Shanghai's urban forest using Landsat ETM+ and inventory data. *Urban For. Urban Green*. **2020**, *51*, 126655. [CrossRef]

30.   Ren, Z.; Zheng, H.; He, X.; Zhang, D.; Yu, X.; Shen, G. Spatial estimation of urban forest structures with Landsat TM data and field measurements. *Urban For. Urban Green*. **2015**, *14*, 336–344. [CrossRef]

31.   Moser, G.; Serpico, S.B.; Benediktsson, J.A. Land-cover mapping by Markov modeling of spatial–contextual information in very-high-resolution remote sensing images. *Proc. IEEE* **2012**, *101*, 631–651. [CrossRef]

32.   Praticò, S.; Solano, F.; Di Fazio, S.; Modica, G. Machine Learning Classification of Mediterranean Forest Habitats in Google Earth Engine Based on Seasonal Sentinel-2 Time-Series and Input Image Composition Optimisation. *Remote Sens*. **2021**, *13*, 586.[CrossRef]

33.   Fassnacht, F.E.; Latifi, H.; Stereńczak, K.; Modzelewska, A.; Lefsky, M.; Waser, L.; Straub, C.; Ghosh, A. Review of studies on tree species classification from remotely sensed data. *Remote Sens. Environ*. **2016**, *186*, 64–87. [CrossRef]

34.   Van Ewijk, K.Y.; Randin, C.F.; Treitz, P.M.; Scott, N.A. Predicting fine-scale tree species abundance patterns using biotic variables derived from LiDAR and high spatial resolution imagery. *Remote Sens. Environ*. **2014**, *150*, 120–131. [CrossRef]

35.   Chambers, D.; Périé, C.; Casajus, N.; De Blois, S. Challenges in modelling the abundance of 105 tree species in eastern North America using climate, edaphic, and topographic variables. *For. Ecol. Manag*. **2013**, *291*, 20–29. [CrossRef]

36.   Choudhury, A.M.; Marcheggiani, E.; Despini, F.; Costanzini, S.; Rossi, P.; Galli, A.; Teggi, S. Urban Tree Species Identification and Carbon Stock Mapping for Urban Green Planning and Management. *Forests* **2020**, *11*, 1226. [CrossRef]

37.   Vauhkonen, J.; Ørka, H.O.; Holmgren, J.; Dalponte, M.; Heinzel, J.; Koch, B. *Tree Species Recognition Based on Airborne Laser Scanning and Complementary Data Sources*; Springer: Berlin/Heidelberg, Germany, 2013; Volume 27, pp. 135–156.

38.   Ørka, H.O.; Dalponte, M.; Gobakken, T.; Næsset, E.; Ene, L.T. Characterizing forest species composition using multiple remote sensing data sources and inventory approaches. *Scand. J. For. Res*. **2013**, *28*, 677–688. [CrossRef]

39.   Adelabu, S.; Mutanga, O.; Adam, E.E.; Cho, M.A. Exploiting machine learning algorithms for tree species

classification in a semiarid woodland using RapidEye image. *J. Appl. Remote Sens*. **2013**, *7*, 073480. [CrossRef]

40.   Carleer, A.; Wolff, E. Exploitation of Very High Resolution Satellite Data for Tree Species Identification. *Photogramm. Eng. Remote Sens*. **2004**, *70*, 135–140. [CrossRef]

41.   Ghosh, A.; Fassnacht, F.E.; Joshi, P.K.; Koch, B. A framework for mapping tree species combining hyperspectral and LiDAR data: Role of selected classifiers and sensor across three spatial scales. *Int. J. Appl. Earth Obs. Geoinf*. **2014**, *26*, 49–63. [CrossRef]

42.   Jensen, R.R.; Hardin, P.J.; Hardin, A.J. Classification of urban tree species using hyperspectral imagery. *Geocarto Int*. **2012**, *27*, 443–458. [CrossRef]

43.   Somers, B.; Asner, G.P. Tree species mapping in tropical forests using multi-temporal imaging spectroscopy: Wavelength adaptive spectral mixture analysis. *Int. J. Appl. Earth Obs. Geoinf*. **2014**, *31*, 57–66. [CrossRef]

44.   Qian, Y.; Zhou, W.; Pickett, S.T.A.; Yu, W.; Xiong, D.; Wang, W.; Jing, C. Integrating structure and function: Mapping the hierarchical spatial heterogeneity of urban landscapes. *Ecol. Process*. **2020**, *9*, 1–11. [CrossRef]

45.   Zhou, W.; Troy, A. An object-oriented approach for analysing and characterizing urban landscape at the parcel level. *Int. J. Remote Sens*. **2008**, *29*, 3119–3135. [CrossRef]

46.   Ouma, Y.O.; Tateishi, R. Urban-trees extraction from Quickbird imagery using multiscale spectex-filtering and non-parametric classification. *ISPRS J. Photogramm. Remote Sens*. **2008**, *63*, 333–351. [CrossRef]

47.   Lee, D.S.; Shan, J.; Bethel, J.S. Class-Guided Building Extraction from Ikonos Imagery. *Photogramm. Eng. Remote Sens*. **2003**, *69*, 143–150. [CrossRef]

48.   Johnson, B.A.; Jozdani, S.E. Identifying Generalizable Image Segmentation Parameters for Urban Land Cover Mapping through Meta-Analysis and Regression Tree Modeling. *Remote Sens*. **2018**, *10*, 73. [CrossRef]

49.   Degerickx, J.; Hermy, M.; Somers, B. Mapping Functional Urban Green Types Using High Resolution Remote Sensing Data. *Sustainability* **2020**, *12*, 2144. [CrossRef]

50.   Puissant, A.; Rougier, S.; Stumpf, A. Object-oriented mapping of urban trees using Random Forest classifiers. *Int. J. Appl. Earth Obs. Geoinf*. **2014**, *26*, 235–245. [CrossRef]

51.   Pu, R.; Landry, S. Mapping urban tree species by integrating multi-seasonal high resolution pléiades satellite imagery with airborne LiDAR data. *Urban For. Urban Green*. **2020**, *53*, 126675. [CrossRef]

52.   Pu, R.; Landry, S. A comparative analysis of high spatial resolution IKONOS and WorldView-2 imagery for mapping urban tree species. *Remote Sens. Environ*. **2012**, *124*, 516–533. [CrossRef]

53.   Mitchell, M.G.; Johansen, K.; Maron, M.; McAlpine, C.; Wu, D.; Rhodes, J.R. Identification of fine scale and landscape scale drivers of urban aboveground carbon stocks using high-resolution modeling and mapping. *Sci. Total. Environ*. **2018**, *622-623*, 57–70.[CrossRef] [PubMed]

54.   Caynes, R.J.C.; Mitchell, M.G.E.; Wu, D.S.; Johansen, K.; Rhodes, J.R. Using high-resolution LiDAR data to quantify the three-dimensional structure of vegetation in urban green space. *Urban Ecosyst*. **2016**, *19*, 1749–1765. [CrossRef]

55.   Birdal, A.C.; Avdan, U.; Türk, T. Estimating tree heights with images from an unmanned aerial vehicle. *Geomat. Nat. Hazards Risk* **2017**, *8*, 1144–1156. [CrossRef]

56.   Alonzo, M.; Bookhagen, B.; Roberts, D.A. Urban tree species

mapping using hyperspectral and lidar data fusion. *Remote Sens. Environ*. **2014**, *148*, 70–83. [CrossRef]

57.   Kim, S.; McGaughey, R.J.; Andersen, H.-E.; Schreuder, G. Tree species differentiation using intensity data derived from leaf-on and leaf-off airborne laser scanner data. *Remote Sens. Environ*. **2009**, *113*, 1575–1586. [CrossRef]

58.   Plowright, A.A.; Coops, N.C.; Eskelson, B.N.; Sheppard, S.R.; Aven, N.W. Assessing urban tree condition using airborne light detection and ranging. *Urban For. Urban Green*. **2016**, *19*, 140–150. [CrossRef]

59.   Kim, S.; Hinckley, T.; Briggs, D. Classifying individual tree genera using stepwise cluster analysis based on height and intensity metrics derived from airborne laser scanner data. *Remote Sens. Environ*. **2011**, *115*, 3329–3342. [CrossRef]

60.   Ørka, H.O.; Næsset, E.; Bollandsås, O.M. Classifying species of individual trees by intensity and structure features derived from airborne laser scanner data. *Remote Sens. Environ*. **2009**, *113*, 1163–1174. [CrossRef]

61.   Yao, W.; Krzystek, P.; Heurich, M. Tree species classification and estimation of stem volume and DBH based on single tree extraction by exploiting airborne full-waveform LiDAR data. *Remote Sens. Environ*. **2012**, *123*, 368–380. [CrossRef]

62.   Myeong, S.; Nowak, D.J.; Hopkins, P.F.; Brock, R.H. Urban cover mapping using digital, high-spatial resolution aerial imagery. *Urban Ecosyst*. **2001**, *5*, 243–256. [CrossRef]

63.   Qian, Y.; Zhou, W.; Nytch, C.J.; Han, L.; Li, Z. A new index to differentiate tree and grass based on high resolution image and object-based methods. *Urban For. Urban Green*. **2020**, *53*, 126661. [CrossRef]

64.   Azeez, O.S.; Pradhan, B.; Shafri, H.Z.M.; Shukla, N.; Lee, C.H.; Rizeei, H.M. Modeling of

This mapping approach could be an efficient tool in CS mapping that will assist urban planners in ensuring proper utilization of the available green spaces considering other valuable prospects of tree species mapping in a complex city environment.

CO emissions from traffic vehicles using artificial neural networks. *Appl. Sci.* **2019**, *9*, 313. [CrossRef]

65. Wilkes, P.; Disney, M.; Vicari, M.; Calders, K.; Burt, A. Estimating urban above ground biomass with multi-scale LiDAR. *Carbon Balance Manag.* **2018**, *13*, 10. [CrossRef]

66. Zhu, Z.; Zhou, Y.; Seto, K.C.; Stokes, E.C.; Deng, C.; Pickett, S.T.; Taubenböck, H. Understanding an urbanizing planet: Strategic directions for remote sensing. *Remote Sens. Environ.* **2019**, *228*, 164–182. [CrossRef]

67. Maynard, C.L.; Lawrence, R.L.; Nielsen, G.A.; Decker, G. Modeling Vegetation Amount Using Bandwise Regression and Ecological Site Descriptions as an Alternative to Vegetation Indices. *GISci. Remote Sens.* **2007**, *44*, 68–81. [CrossRef]

68. Kankare, V.; Vastaranta, M.; Holopainen, M.; Räty, M.; Yu, X.; Hyyppä, J.; Hyyppä, H.; Alho, P.; Viitala, R. Retrieval of Forest Aboveground Biomass and Stem Volume with Airborne Scanning LiDAR. *Remote Sens.* **2013**, *5*, 2257–2274. [CrossRef]

69. Wannasiri, W.; Nagai, M.; Honda, K.; Santitamnont, P.; Miphokasap, P. Extraction of Mangrove Biophysical Parameters Using Airborne LiDAR. *Remote Sens.* **2013**, *5*, 1787–1808. [CrossRef]

70. Lu, D. The potential and challenge of remote sensing-based biomass estimation. *Int. J. Remote Sens.* **2006**, *27*, 1297–1328. [CrossRef]

71. Foody, G.M.; Boyd, D.S.; Cutler, M. Predictive relations of tropical forest biomass from Landsat TM data and their transferability between regions. *Remote Sens. Environ.* **2003**, *85*, 463–474. [CrossRef]

72. Kobayashi, S.; Omura, Y.; Sanga-Ngoie, K.; Widyorini, R.; Kawai, S.; Supriadi, B.; Yamaguchi, Y. Characteristics of Decomposition Powers of L-Band Multi-Polarimetric SAR in Assessing Tree Growth of Industrial Plantation Forests in the Tropics. *Remote Sens.* **2012**, *4*, 3058–3077. [CrossRef]

73. Clewley, D.; Lucas, R.; Accad, A.; Armston, J.; Bowen, M.; Dwyer, J.; Pollock, S.; Bunting, P.; McAlpine, C.; Eyre, T.; et al. An Approach to Mapping Forest Growth Stages in Queensland, Australia through Integration of ALOS PALSAR and Landsat Sensor Data. *Remote Sens.* **2012**, *4*, 2236–2255. [CrossRef]

74. Robinson, C.; Saatchi, S.; Neumann, M.; Gillespie, T. Impacts of Spatial Variability on Aboveground Biomass Estimation from L- Band Radar in a Temperate Forest. *Remote Sens.* **2013**, *5*, 1001–1023. [CrossRef]

75. Zheng, D.; Rademacher, J.; Chen, J.; Crow, T.; Bresee, M.; Le Moine, J.; Ryu, S.-R. Estimating aboveground biomass using Landsat 7 ETM+ data across a managed landscape in northern Wisconsin, USA. *Remote Sens. Environ.* **2004**, *93*, 402–411. [CrossRef]

76. Coulibaly, L.; Migolet, P.; Adegbidi, H.; Fournier, R.; Hervet, E. Mapping Aboveground Forest Biomass from Ikonos Satellite Image and Multi-Source Geospatial Data using Neural Networks and a Kriging Interpolation. *Int. Geosci. Remote Sens. Symp.* **2008**, *3*, III-298. [CrossRef]

77. Castel, T. Retrieval biomass of a large Venezuelan pine plantation using JERS-1 SAR data. Analysis of forest structure impact on radar signature. *Remote Sens. Environ.* **2002**, *79*, 30–41. [CrossRef]

78. Wijaya, A.; Gloaguen, R. Fusion of ALOS Palsar and Landsat ETM data for land cover classification and biomass modeling using non-linear methods. *Int. Geosci. Remote Sens. Symp.* **2009**, *3*, III-581. [CrossRef]

79. Simple Random Sampling of Individual Items in the Absence of a Sampling Frame that Lists the Individuals|New Zealand Journal of Forestry Science|Full Text. Available online: https://nzjforestryscience.springeropen.com/articles/10.1186/s40490-016-0071-1 (accessed on 24 May 2021).

80. West, P.W. Simple random sampling of individual items in the absence of a sampling frame that lists the individuals. *N. Z. J. For. Sci.* **2016**, *46*, 1–7. [CrossRef]

81. Gregoire, T.G.; Valentine, H.T. *Sampling Strategies for Natural Resources and the Environment*; Chapman and Hall/CRC: Boca Raton, FL, USA, 2007.

82. Pinkham, R.S. An Efficient Algorithm for Drawing a Simple Random Sample. *J. R. Stat. Soc. Ser. C Appl. Stat.* **1987**, *36*, 370.[CrossRef]

83. Nikon|News|Nikon Introduces New Laser Rangefinder "Forestry 550". Available online: https://www.nikon.com/news/2008 /0924_forestry_02.htm (accessed on 16 November 2020).

84. Degerickx, J.; Roberts, D.; McFadden, J.; Hermy, M.; Somers, B. Urban tree health assessment using

airborne hyperspectral and LiDAR imagery. *Int. J. Appl. Earth Obs. Geoinf.* **2018**, *73*, 26–38. [CrossRef]

85. Solano, F.; Di Fazio, S.; Modica, G. A methodology based on GEOBIA and WorldView-3 imagery to derive vegetation indices at tree crown detail in olive orchards. *Int. J. Appl. Earth Obs. Geoinf.* **2019**, *83*, 101912. [CrossRef]

86. Gilbertson, J.K.; Kemp, J.; van Niekerk, A. Effect of pan-sharpening multi-temporal Landsat 8 imagery for crop type differentiation using different classification techniques. *Comput. Electron. Agric.* **2017**, *134*, 151–159. [CrossRef]

87. Karakus, P.; Karabork, H. Effect of pansharpened image on some of pixel based and object based classification accuracy. *ISPRS Int. Arch. Photogramm. Remote Sens. Spat. Inf. Sci.* **2016**, *XLI-B7*, 235–239. [CrossRef]

88. Padwick, C.; Deskevich, M.; Pacifici, F.; Smallwood, S. WorldView-2 Pan-Sharpening. In Proceedings of the ASPRS 2010 Annual Conference, San Diego, CA, USA, 26–30 April 2010; Volume 2630, pp. 1–14.

89. Geopunt.be—The Flemish Geoportal|Con Terra. Available online: https://www.con-terra.com/casestudies/geopuntbe-flemish-geoportal (accessed on 9 January 2021).

90. ERDAS IMAGINE: World-Class Remote Sensing Software|Hexagon Geospatial. Available online: https://www.hexagongeospatial. com/products/power-portfolio/erdas-imagine/erdas-imagine-remote-sensing-software-package (accessed on 9 January 2021).

91. UrbIS Download. Available online: http://urbisdownload.gis.irisnet.be/en/temporality/ (accessed on 16 November 2020).

92. Jebur, M.N.; Shafri, H.Z.M.; Pradhan, B.; Tehrany, M.S. Per-pixel and object-oriented classification methods for

mapping urban land cover extraction using SPOT 5 imagery. *Geocarto Int.* **2013**, *29*, 792–806. [CrossRef]

93. Wang, L.; Sousa, W.P.; Gong, P. Integration of object-based and pixel-based classification for mapping mangroves with IKONOS imagery. *Int. J. Remote Sens.* **2004**, *25*, 5655–5668. [CrossRef]

94. Makinde, E.O.; Salami, A.; Olaleye, J.B.; Okewusi, O.C. Object Based and Pixel Based Classification Using Rapideye Satellite Imager of ETI-OSA, Lagos, Nigeria. *Geoinformatics FCE CTU* **2016**, *15*, 59–70. [CrossRef]

95. Blaschke, T.; Lang, S.; Lorup, E.; Strobl, J.; Zeil, P. Object-oriented image processing in an integrated GIS/remote sensing environment and perspectives for environmental applications. *Environ. Inf. Plan. Politics Public* **2000**, *2*, 555–570.

96. Estoque, R.C.; Murayama, Y.; Akiyama, C. Pixel-based and object-based classifications using high- and medium-spatial-resolution imageries in the urban and suburban landscapes. *Geocarto Int.* **2015**, *30*, 1113–1129. [CrossRef]

97. Li, X.; Meng, Q.; Gu, X.; Jancsó, T.; Yu, T.; Wang, K.; Mavromatis, S. A hybrid method combining pixel-based and object-oriented methods and its application in Hungary using Chinese HJ-1 satellite images. *Int. J. Remote Sens.* **2013**, *34*, 4655–4668. [CrossRef]

98. Jabari, S.; Zhang, Y. Very High Resolution Satellite Image Classification Using Fuzzy Rule-Based Systems. *Algorithms* **2013**, *6*, 762–781. [CrossRef]

99. Platt, R.V.; Rapoza, L. An Evaluation of an Object-Oriented Paradigm for Land Use/Land Cover Classification*. *Prof. Geogr.* **2008**, *60*, 87–100. [CrossRef]

100. Wieland, M.; Pittore, M. Performance Evaluation of Machine

Learning Algorithms for Urban Pattern Recognition from Multi-spectral Satellite Images. *Remote Sens.* **2014**, *6*, 2912–2939. [CrossRef]

101. Gao, Y.; Mas, J.F. 2008. A Comparison of the Performance of Pixel Based and Object Based Classifications over Images with Various Spatial Resolutions. Available online: https://medwelljournals.com/abstract/?doi=ojesci.2008.27.35 (accessed on 24 May 2021).

102. Han, R.; Liu, P.; Wang, G.; Zhang, H.; Wu, X. Advantage of Combining OBIA and Classifier Ensemble Method for Very High-Resolution Satellite Imagery Classification. *J. Sens.* **2020**, *2020*, *1–15*. [CrossRef]

103. Hossain, M.D.; Chen, D. Segmentation for Object-Based Image Analysis (OBIA): A review of algorithms and challenges from remote sensing perspective. ISPRS J. Photogramm. *Remote Sens.* **2019**, *150*, 115–134. [CrossRef]

104. Kucharczyk, M.; Hay, G.; Ghaffarian, S.; Hugenholtz, C. Geographic Object-Based Image Analysis: A Primer and Future Directions. *Remote Sens.* **2020**, *12*, 2012. [CrossRef]

105. Blaschke, T. Object based image analysis for remote sensing. ISPRS J. Photogramm. *Remote Sens.* **2010**, *65*, 2–16. [CrossRef]

106. Fu, B.; Wang, Y.; Campbell, A.; Li, Y.; Zhang, B.; Yin, S.; Xing, Z.; Jin, X. Comparison of object-based and pixel-based Random Forest algorithm for wetland vegetation mapping using high spatial resolution GF-1 and SAR data. *Ecol. Indic.* **2017**, *73*, 105–117.[CrossRef]

107. Duro, D.C.; Franklin, S.; Dubé, M.G. A comparison of pixel-based and object-based image analysis with selected machine learning algorithms for the classification of agricultural landscapes using SPOT-5 HRG imagery. *Remote Sens. Environ.* **2012**, *118*, 259–272.[CrossRef]

108. Myint, S.W.; Gober, P.; Brazel, A.; Grossman-Clarke, S.; Weng, Q. Per-pixel vs. object-based classification of urban land cover extraction using high spatial resolution imagery. *Remote Sens. Environ.* **2011**, *115*, 1145–1161. [CrossRef]

109. Martins, V.S.; Kaleita, A.L.; Gelder, B.K.; da Silveira, H.L.; Abe, C.A. Exploring multiscale object-based convolutional neural network (multi-OCNN) for remote sensing image classification at high spatial resolution. ISPRS J. Photogramm. *Remote Sens.* **2020**, *168*, 56–73. [CrossRef]

110. Su, T.; Liu, T.; Zhang, S.; Qu, Z.; Li, R. Machine learning-assisted region merging for remote sensing image segmentation. ISPRS J. Photogramm. *Remote Sens.* **2020**, *168*, 89–123. [CrossRef]

111. De Pinho, C.M.D.; Fonseca, L.M.G.; Korting, T.S.; Almeida, C.; Kux, H.J.H. Land-cover classification of an intra-urban environment using high-resolution images and object-based image analysis. *Int. J. Remote Sens.* **2012**, *33*, 5973–5995. [CrossRef]

112. AGD. *ECognition Version 5 Object Oriented Image Analysis User Guide*; AGD: Munich, Germany, 2005.

113. Basic Rule Set Editing. Available online: https://docs. ecognition.com/v9.5.0/eCognition_ documentation/UserGuideDeveloper/ 4BasicRuleSetEditing.htm (accessed on 17 November 2020).

114. El-Naggar, A.M. Determination of optimum segmentation parameter values for extracting building from remote sensing images. *Alex. Eng. J.* **2018**, *57*, 3089–3097. [CrossRef]

115. Huang, J.; Zhang, X.; Xin, Q.; Sun, Y.; Zhang, P. Automatic building extraction from high-resolution aerial images and LiDAR data using gated residual refinement network. ISPRS J. Photogramm. *Remote Sens.* **2019**, *151*, 91–105. [CrossRef]

116. Multiresolution Segmentation: An Optimization Approach . . . / Multiresolution-Segmentation-An-Optimization-Approach.pdf/PDF4PRO. Available online: https://pdf4pro.com/ view/multiresolution-segmentation-an-optimization-approach-598443. html (accessed on 19 May 2021).

117. Modica, G.; Messina, G.; De Luca, G.; Fiozzo, V.; Praticò, S. Monitoring the vegetation vigor in heterogeneous citrus and olive orchards. A multiscale object-based approach to extract trees' crowns from UAV multispectral imagery. *Comput. Electron. Agric.* **2020**, *175*, 105500. [CrossRef]

118. Benz, U.C.; Hofmann, P.; Willhauck, G.; Lingenfelder, I.; Heynen, M. Multi-resolution, object-oriented fuzzy analysis of remote sensing data for GIS-ready information. ISPRS J. Photogramm. *Remote Sens.* **2004**, *58*, 239–258. [CrossRef]

119. Carneiro, F.M.; Furlani, C.E.A.; Zerbato, C.; De Menezes, P.C.; Gírio, L.A.D.S. Correlations among vegetation indices and peanut traits during different crop development stages. *Eng. Agríc.* **2019**, *39*, 33–40. [CrossRef]

120. Blanzieri, E.; Melgani, F. Nearest Neighbor Classification of Remote Sensing Images with the Maximal Margin Principle. IEEE Trans. Geosci. *Remote Sens.* **2008**, *46*, 1804–1811. [CrossRef]

121. Blunt, W. *Linnaeus*: *The Compleat Naturalist*; Princeton University Press: Princeton, NJ, USA, 2001; Available online: https: //www.worldcat.org/ title/linnaeus-the-compleat-naturalist/ oclc/1159631211?referer=di&ht=edition (accessed on 24 May 2021).

122. Gupta, D.L.; Malviya, A.K.; Singh, S. Performance Analysis of Classification Tree Learning Algorithms. *Int. J. Comput. Appl.* **2012**, *55*, 39–44. [CrossRef]

123. Immitzer, M.; Vuolo, F.; Atzberger, C. First Experience with Sentinel-2 Data for Crop and Tree Species Classifications in Central Europe. *Remote Sens.* **2016**, *8*, 166. [CrossRef]

124. So-In, C.; Mongkonchai, N.; Aimtongkham, P.; Wijitsopon, K.; Rujirakul, K. An evaluation of data mining classification models for network intrusion detection. In Proceedings of the 2014 Fourth International Conference on Digital Information and Communication Technology and its Applications (DICTAP), Bangkok, Thailand, 6–8 May 2014; pp. 90–94.

125. Foody, G.M. Assessing the Accuracy of Remotely Sensed Data: Principles and Practices. *Photogramm. Rec.* **2010**, *25*, 204–205.[CrossRef]

126. Helldén, *U. A Test of Landsat-2 Imagery and Digital Data for Thematic Mapping Illustrated by an Environmental Study in Northern Kenya*; Lund University: Lund, Sweden, 1980.

127. Cohen, J. Weighted kappa: Nominal scale agreement provision for scaled disagreement or partial credit. *Psychol. Bull.* **1968**, *70*, 213–220. [CrossRef] [PubMed]

128. Banko, G. *A Review of Assessing the Accuracy of Classifications of Remotely Sensed Data and of Methods Including Remote Sensing Data in Forest Inventory*; IIASA Interim Report; IIASA: Laxenburg, Austria, 1998; IR-98-081.

129. Gallaun, H.; Zanchi, G.; Nabuurs, G.J.; Hengeveld, G.; Schardt, M.; Verkerk, P.J. EU-wide maps of growing stock and above-ground biomass in forests based on remote sensing and field measurements. *For. Ecol. Manag.* **2010**, *260*, 252–261. [CrossRef]

130. Cairns, M.A.; Brown, S.; Helmer, E.H.; Baumgardner, G.A. Root biomass allocation in the world's upland forests. *Oecologia* **1997**, *111*, 1–11. [CrossRef] [PubMed]

131. Fonton, N.H.; Medjibé, V.; Djomo, A.; Kondaoulé, J.; Rossi, V.; Ngomanda, A.; Maïdou, H. Analyzing Accuracy

of the Power Functions for Modeling Aboveground Biomass Prediction in Congo Basin Tropical Forests. *Open J. For.* **2017**, *07*, 388–402.[CrossRef]

132.   Kumar, L.; Sinha, P.; Taylor, S.; AlQurashi, A.F. Review of the use of remote sensing for biomass estimation to support renewable energy generation. J. *Appl. Remote Sens.* **2015**, *9*, 097696. [CrossRef]

133.   Tabacchi, G.; Cosmo, D.; Gasparini, L. Aboveground tree volume and Phytomass Prediction Equations for Forest Species in Italy. *Eur. J. For. Res.* **2011**, *130*, 911–934. [CrossRef]

134.   Goslee, K.; Walker, S.M.; Grais, A.; Murray, L.; Casarim, F.; Brown, *S. Leaf Technical Guidance Series for the Development of a Forest Carbon Monitoring System for REDD+: Module C-CS: Calculations for Estimating Carbon Stocks*; Winrock International: Morrilton, AR, USA, 2010.

135.   Biomass, B.S.E. And Biomass Change of Tropical Forests: A Primer. *Rome FAO For. Pap.* **1986**, *134.*

136.   Losi, C.J.; Siccama, T.G.; Condit, R. Analysis of Alternative Methods for Estimating Carbon Stock in Young Tropical Plantatiions. *For. Ecol. Manag.* **2003**, *184*, 355–368. [CrossRef]

137.   Vashum, K.T.; Jayakumar, S. Methods to Estimate Above-Ground Biomass and Carbon Stock in Natural Forests-a Review. *J. Ecosyst. Ecography* **2012**, *2*, 1–7. [CrossRef]

138.   Whittaker, R.H. Carbon in the Biota. In Woodwell GM, Pecan EV, Carbon in the biosphere. In Proceedings of the 24th Brookhaven Symposium in Biology, New York, NY, USA, 16–18 May 1972; pp. 281–302.

139.   Food and Agriculture Organization. *Food and Agriculture Organization of the United Nations. Retrieved*; Food and Agriculture Organization: Rome, Italy, 2010; p. 2012.

140.   Vicharnakorn, P.; Shrestha, R.P.; Nagai, M.; Salam, A.P.; Kiratiprayoon, S. Carbon Stock Assessment Using Remote Sensing and Forest Inventory Data in Savannakhet, Lao PDR. *Remote Sens.* **2014**, *6*, 5452–5479. [CrossRef]

141.   Panel, I. *On Climate Change (IPCC)*; Cambridge University Press: Cambridge, UK, 2007.

142.   Rahetlah, B.V.; Salgado, P.; Andrianarisoa, B.; Tillard, E.; Razafindrazaka, H.; Le Mezo, L.; Ramalanjaona, V.L. 2014. Relationship between Normalized Difference Vegetation Index (NDVI) and Forage Biomass Yield in the Vakinankaratra Region, Madagascar.

143.   Goswami, S.; Gamon, J.; Vargas, S.; Tweedie, C. Relationships of NDVI, Biomass, and Leaf Area Index (LAI) for Six Key Plant Species in Barrow, Alaska. *PeerJ Prepr.* **2015**, *19*.

144.   Coelho, A.P.; Rosalen, D.L.; De Faria, R.T. Vegetation indices in the prediction of biomass and grain yield of white oat under irrigation levels. *Pesquisa Agropecuária Tropical* **2018**, *48*, 109–117. [CrossRef]

145.   Jung, M. 2013. LecoS-A QGIS plugin for automated landscape ecology analysis (No. e116v2). *PeerJ* **2013**. [CrossRef]

The paper originally published in Forests 2021, 12,692. https://doi.org/10.3390/ f12060692 has been republished wth authors' permission.

To be concluded in the next issue. ◣

Tech Mahindra and Cisco join hands

Tech Mahindra has collaborated with Cisco to drive the infrastructure modernization of optical transport networks with the introduction of Cisco routed optical networking. The collaboration aims to simplify the Internet transport networks by leveraging state-of-the-art optical and routing technologies to converge services over an IP Infrastructure enabling a high degree of automation. The collaboration will empower service providers to reduce their operational expenses and their total cost of ownership.

Meter-level location accuracy for smartphones by Qualcomm and Trimble

Trimble and Qualcomm Technologies, Inc. have announced the availability of Trimble RTX GNSS technology for Snapdragon 8 Gen 1 and Snapdragon 888 Mobile Platforms. This technology enables superior location capabilities in premium Android smartphones worldwide.

Coupling the Trimble RTX technology with premium Snapdragon Mobile Platforms supercharges Android phones' positioning capabilities. This will enable smartphone manufacturers, service providers and application developers using Snapdragon to provide mobile users with robust meter-level accuracy (or about 3 feet) when used with a Trimble RTX-based correction service. This represents a 5x improvement in location accuracy compared to typical accuracy available today. *www.trimble.com*

DeepRoute.ai to integrate NVIDIA DRIVE Hyperion

DeepRoute.ai will integrate the NVIDIA DRIVE Hyperion AVcomputing architecture into its Level 4 autonomous driving solution. With this upgrade, DeepRoute-Driver 2.0 will meet automotive-grade requirements and advance the company's plans to bring production-ready solutions to the consumer market. Road testing will start during Q2 of 2022, with mass production expected to begin in Q1 of 2023. ◣

Assessment of geo-hazards in Nepal

Synspective Inc., under the supervision of the World Bank and National Disaster Risk Reduction and Management Authority (NDRRMA), Government of Nepal, investigated the land displacement hazards in the upstream part of the Melamchi River, Nepal in response to the destructive flood disaster that occurred in June'21. The results demonstrated that Synthetic Aperture Radar (SAR) data and time-series interferometric SAR (InSAR) analysis-based Earth observation techniques have the capabilities to offer a more cost-saving alternative to periodically monitor slopes with susceptibility and identify the potential precursors of slow-evolving failure conditions.

Using data gathered by the European Space Agency's SAR satellite, Synspective's Land Displacement Monitoring (LDM) service monitored over 400 km2 of slope area in the upstream proximity of the Melamchi River. The analysis results were used to support the authorities' work in managing slope susceptibility risk in the region. In addition to residential communities, critical facilities and lifeline infrastructure are also present in the region including the Headworks of the Kathmandu Valley Water Supply Improvement Project financed by the ADB. *https://synspective.com*

Project to support EV chargepoint infrastructure in UK

The UK Geospatial Commission has launched a discovery project to explore how location data can be better utilised to support planning and delivery of electric vehicle charge points by local authorities.

This project will support the approach set out in the government's Electric Vehicle Infrastructure Strategy, published by the Department for Transport, which focuses on enabling the rollout of a robust EV charging infrastructure network by 2030. Setting out a vision and approach for EV infrastructure roll-

out and expectations of key stakeholders, the Strategy identifies that addressing barriers to data sharing will be important to enable decision making. *www.gov.uk*

White House launches COVID.gov

The White House launched COVID.gov, a new one-stop shop website to help all people in the United States gain even better access to lifesaving tools like vaccines, tests, treatments, and masks, as well as get the latest updates on COVID-19 in their area. As part of COVID.gov, a new Test-to-Treat locator will help people access pharmacies and community health centers across the nation where people can get tested for COVID-19 and receive appropriate treatments if they need them.

Built upon GIS and mapping technology from Esri, which is used for the Johns Hopkins worldwide COVID-19 map, the COVID-19 Test-to-Treat locator provides locations for people to get tested – and if they test positive and are eligible for treatment – receive a prescription from an on-site or affiliated health care provider, and have their prescription filled all at one convenient location.

ABB inaugurates its Innovation Center in India

ABB has inaugurated a new and expanded R & D and engineering facility, the ABB Innovation Centre (AIC) in Bengaluru, India. This state-of-the-art facility is one of its largest globally and serves as the backbone for technology developments to accelerate innovation. It houses 2500 diverse technologists including engineers, principal and data scientists, architects, domain and analytics specialists, programmers, and developers. *https://global.abb/group/en*

India's second space training center opens in Jammu

ISRO, Department of Space, and Central University of Jammu (CUJ) has jointly established a Space science center for carrying out research in

Space science and technology in the Central University campus, Jammu. The Centre is named after the renowned Space Scientist, teacher and former Chairman, ISRO, Prof. Satish Dhawan, who hailed from Jammu & Kashmir.

The Satish Dhawan Space Science Centre was inaugurated by Dr. Jitendra Singh, Minister of State (MoS) for Space, in the presence of Somanath S, Chairman, ISRO/Secretary DOS, Dr. K. Radhakrishnan Former Chairman, ISRO & Member, Space Commission and Prof. Sanjeev Jain, VC-CUJ, on March 12, 2022.

The Centre houses different labs/facilities related to geospatial data analysis, materials, astrophysics, natural disasters and avionics.

Fugro supports NIOT's coastal community development plan

India's National Institute of Ocean Technology (NIOT) has commissioned Fugro to carry out a bathymetric survey along the Andhra Pradesh coast in south-eastern India. The survey will facilitate the Indian Government's plans to develop and manage the exclusive economic zone (EEZ) to benefit the coastal community and protect marine living resources. The data will also be used for a range of scientific research projects and coastal resilience studies like assessment of coastal vulnerabilities and geohazard potential and ocean climate change.

The six-month project started in November 2021. Fugro will survey around 56,000-line kilometres of coastline in total, collecting bathymetric data in water depths between High Tide Line (HTL) and 30 m. To gather insights about the seabed, its specialist team is using a shallow-water boat equipped with a dual frequency echosounder and a DGPS for data acquisition. For safe and efficient surveying in very shallow water (up to 5 m) and the surf zone area, the team is going to use jet ski equipped with Differential Global Positioning System (DGPS) and a single beam echosounder.

Real-time kinematic positioning (RTK) technology is being used for topography survey. *www.fugro.com*

UKHO signs collaboration agreement with The Nippon Foundation–GEBCO Seabed 2030 Project

The UK Hydrographic Office (UKHO) has signed a MOU with The Nippon Foundation-GEBCO Seabed 2030 Project, which will see the parties work together to advance the industry's understanding of ocean bathymetry, and in support of the Decade of Ocean Science for Sustainable Development.

Seabed 2030 – a flagship program of the Ocean Decade – is a collaborative project between The Nippon Foundation and the General Bathymetric Chart of the Oceans (GEBCO) with the goal of the complete mapping of the world's oceans by 2030, as well as compiling all bathymetric data into the freely available GEBCO Ocean Map. GEBCO is a joint program of the International Hydrographic Organization (IHO) and the Intergovernmental Oceanographic Commission (IOC), and is the only organization with a mandate to map the entire ocean floor.

As part of its official partnership with Seabed 2030, the UKHO will provide bathymetric gridded map products to be used by the project within the GEBCO gridded bathymetric data set. UKHO will also share and promote methods and best practices in technological innovation, infrastructure and solutions for ocean mapping and bathymetric data management. *https://seabed2030.org*

Infrastructure–based 3D perception software by Seoul Robotics

Seoul Robotics has introduced an infrastructure-based version of its patented 3D perception software. SENSR-I processes data captured by 3D sensors over large spaces to provide high-resolution environmental insights, enabling a wide range of applications to inform organizations on operational efficiencies, safety enhancements, crowd management and customer experience improvements. Designed for use with 3D sensors that are placed on static infrastructure in both indoor and outdoor applications, SENSR-I is equipped with weather-filtering capabilities to ensure the highest level of accuracy in all conditions, including heavy snow and rain. *www.seoulrobotics.org*

Updated land–cover map with new sets of global data by Esri

Esri in partnership with Impact Observatory and Microsoft, is releasing a globally consistent 2017–2021 global land-use and land-cover map of the world based on the most up-to-date 10-meter Sentinel-2 satellite data. In addition to the new 2021 data, 10-meter land-use and land-cover data for 2017, 2018, 2019, and 2020 is included, illustrating five years of change across the planet.

This digital rendering of earth's surfaces offers detailed information and insights about how land is being used. The map is available online to more than 10 million users of geographic information system (GIS) software through Esri's ArcGIS Living Atlas of the World.

Bentley Education Announces New Student Contest

Bentley Systems, Incorporated has announced Bentley Education's Digital Twin Design Challenge—a student contest that provides an opportunity to reimagine a real-world location with a structure designed with the popular Minecraft video game. Digital twin technology is set to be the next powerful tool for future engineers, and this contest is a unique opportunity for students to explore it in a creative way.

Through the Digital Twin Design Challenge, students have the chance to combine their imagination and creativity by exploring infrastructure digital twins. Students will use Minecraft to take a real-world location and design a new structure within it. In addition to gaining recognition from Bentley Education, the top 20 finalists will receive USD 500 each. The winner chosen by expert judges will receive a prize of USD 5,000, and the winner from the popular vote category will win a prize of USD 2,000. *www.bentley.com*

Integrated support for highway and route shields in TatukGIS SDK

TatukGIS announces integrated support for highway and route shields in its GIS SDK and desktop GIS products. A built-in SVG symbols library provides easy access to shields commonly used to label road and highway maps in the United States, Canada, Europe, and countries around the world. *https://tatukgis.com*

Infotech Partners with cultivate geospatial solutions

Infotech has announced a partnership with Cultivate Geospatial Solutions (CGS) to enhance the incorporation of GIS across Infotech software to track digital as-built data. Through this partnership, the companies will focus on integrating GIS capabilities with project data captured in Infotech solutions and delivering geospatial-based products that support the asset lifecycle. In addition, Cultivate will support Infotech's strategic alliance with Esri, the global leader in location intelligence. *www.infotechinc.com*

XMAP GIS tool aids UK Government

XMAP, the local government GIS service from Geoxphere, now offers a smart, green transport module to help local councils promote Active Travel and secure funding from the Government's £2 billion package to encourage walking and cycling. The XMAP Isochrone tool provides a detailed and visual insight into existing transport infrastructure, assessing accessibility and the local environment to calculate and compare travel times by foot, cycle and car. Its Isochrone tool allows a user to create polygons on a map showing how far it is possible to drive, walk or cycle in a set amount of time. *https://xmap.geoxphere.com*

Terra Drone raises $70M funding

Terra Drone Corporation has raised $70 million (8 billion Japanese yen) in Series B funding with investments from Mitsui & Co., Ltd., SBI Investment Co., Ltd., Tokyu Land Corporation, Kyushu Electric Power T&D, and Seika Corporation. The round also saw the funding by Japan Overseas Infrastructure Investment Corporation for Transport & Urban Development (JOIN) – a public-private infrastructure fund by the Japanese Ministry of Land, Infrastructure, Transport and Tourism (MLIT) – to the newly established joint venture, as well as participation from existing investor Venture Lab Investment. *www.terra-drone.net/global*

FedEx plans to test autonomous drone cargo delivery

FedEx Express is teaming up with Elroy Air, the company building the first end-to-end autonomous vertical take-off and landing (VTOL) aerial cargo system. FedEx Express will develop plans to test Elroy Air's Chaparral autonomous air cargo system within the company's middle-mile logistics operations, moving shipments between sortation locations. This is the latest initiative from FedEx in its effort to explore and adopt emerging technologies across its networks.

Blueprint to build 165 mile drone 'Superhighway'

A consortium led by Reading-based UTM (Unified Traffic Management) software provider Altitude Angel, are planning to build the world's largest and longest network of 'drone superhighways'. The consortium has submitted plans for a '165 miles (265km) drone superhighway' connecting airspace above cities including Reading, Oxford, Milton Keynes, Cambridge, Coventry, and Rugby. Known as Project Skyway, it will enable businesses to develop and grow through the commercialisation of new and innovative drone-based products, processes, and services. *www.altitudeangel.com*

Developing Urban Air Traffic Management System

In 2022, FIXAR becomes a partner of the project Urban Air Traffic Management DEVelOpment & DEMOnstration, led by Istanbul Kultur University Technology Transfer Office. In this project, FIXAR is working together with the project's technical team and providing the full-stack drone solution for flight and system integration, as to demonstrate real time examples of possible solutions. It also takes the role of a lead commercialization partner for RIS (Regional Innovation Scheme) innovation project. *https://fixar.pro*

New lightweight vehicle surveillance system

Teledyne FLIR Defense has launched a new Lightweight Vehicle Surveillance System (LVSS) with revolutionary air domain awareness (ADA) and advanced counter-unmanned aerial system (C-UAS) capabilities. The LVSS ADA C-UAS is an enhanced addition to Teledyne FLIR's field-proven LVSS platform. The new system leverages a powerful combination of 3D radar, EO/IR camera, and RF detection and mitigation sensors to provide early warning alerts and recognition. Threats are detected and displayed simultaneously, showing position and elevation for all radar tracks. *www.flir.com*

eBee TAC drone solution added to Blue UAS

AgEagle Aerial Systems Inc. announced that senseFly, an AgEagle subsidiary, is one of the first eleven vendors to complete the required testing, evaluations and demonstration process to be designated a Blue UAS under the Defense Innovation Unit's Blue sUAS 2.0. As a result, the NDAA-compliant eBee TAC Unmanned Aerial System (UAS), pioneered by senseFly, has been approved by the Defense Innovation Unit (DIU) for procurement by the U.S. Department of Defense (DoD). *www.ageagle.com* ⟍

€2.5 million raised by Neuraspace to prevent satellite collisions

Neuraspace, the developer of an advanced AI-powered Space debris monitoring & satellite collision avoidance platform, has announced that it has raised €2.5 million from Armilar Venture Partners. The company will use these funds to accelerate the commercialisation of its platform.

Neuraspace's proprietary AI technology enables more accurate satellite collision risk prediction and, by applying a data fusion strategy, offers increased robustness and resilience. The platform also automates many of the current manual processes and communications and delivers an end-to-end solution, providing operators with actionable orbital maneuver recommendations to avoid collisions, while delivering valuable insights to various other stakeholders including regulators, insurers and other Space-asset dependent businesses. *https://blog.neuraspace.com*

HFX funds a Satellogic dedicated satellite constellation

HFX has launched the worldwide Ukraine Victory Fund with an initial aim of raising $10 million to dramatically improve Ukraine's access to satellite imagery as it fights Russia's invasion.

The move comes after Ukraine's Ministry of Defence asked for help in raising funds for a Dedicated Satellite Constellation (DSC) – a service provided by Earth observation satellite and data company, Satellogic. It will deploy its DSC service enabling Ukraine to manage a fleet of satellites for encrypted tasking and satellite imagery. It will drastically increase the country's access to high-resolution images and video intelligence. *https://halifaxtheforum.org*

Pixxel announces $25m investment

Pixxel announced a $25 million Series A led by Radical Ventures, a Toronto-based firm known for investing in entrepreneurs that use artificial intelligence to transform

massive industries. The new funding enables Pixxel to expedite production of the world's highest resolution hyperspectral satellite constellation and to offer industry AI-powered insights. *https://timesofindia.indiatimes.com*

SES adds third satellite from Thales Alenia Space

SES has announced that it has ordered SES-26 a fully software-defined geostationary (GEO) satellite from Thales Alenia Space. SES-26 will maintain and expand the wide range of content delivery and connectivity services to broadcasters, media companies, telco operators, internet service providers and governmental organisations across Europe, Africa, the Middle East, and Asia-Pacific. The digital satellite with both Ku-band and C-band frequencies will replace SES's NSS-12 satellite at 57 degrees East, one of SES's longest-held and most valuable orbital positions. From this key location at the crossroads of Europe, the Middle East, Africa and Asia, SES will continue to deliver content and connectivity solutions to some of the world's fastest-growing markets. *www.thalesgroup.com*

OneWeb to resume satellite launches

OneWeb, the low Earth orbit (LEO) satellite communications company and SpaceX entered into an agreement that will enable OneWeb to resume satellite launches. The first launch with SpaceX is anticipated in 2022 and will add to OneWeb's total in-orbit constellation that currently stands at 428 satellites, or 66 percent of the fleet. OneWeb's network will deliver high-speed, low-latency global connectivity. *https://oneweb.net*

NOAA and Partners Discover Wreck of 207-year-old Whaling Ship

NOAA and partners have announced the discovery of the wreck of a 207-year-old whaling ship, called Industry, found on the bottom of the Gulf of Mexico. The remains of the 20-metre long, two-masted wooden brig open a window into a little-known chapter of

American history when descendants of African enslaved people and Native Americans served as essential crew in one of the nation's oldest industries.

With guidance provided via satellite connection from partner scientists on shore, a team aboard NOAA ship Okeanos Explorer piloted a remotely operated vehicle (ROV) to explore the seafloor on 25 February 2022, at a suspected location first spotted by an energy company in 2011 and viewed briefly by an autonomous vehicle in 2017, but never fully examined.

Extra-terrestrial lab launches in South Australia

The Extraterrestrial Environmental Simulation (Exterres) Laboratory is the first of its kind in Australia and will allow researchers to develop new technologies to withstand the harsh deep space environment. Led by University of Adelaide Associate Professor John Culton, the lab will be used to test equipment such as rovers and materials needed for human exploration.

"Understanding how technology will perform when exposed to harsh extra-terrestrial environments is critical to supporting long-term human presence in deep space, specifically the Moon and Mars," said Culton, who is Professor of Off-Earth Resources and the Director of the Andy Thomas Centre for Space Resources.

"Space hardware will be tested in the lab's Regolith Thermal Vacuum Chambers (rTVAC), a nine square metre sealed lunar regolith simulant pit and a 27 square metre sandpit which can be tailored to simulate specific off-world environments."

Hunting for pathogen killing Hawaiian tree using airborne remote sensing

A new study published in Ecological Applications by researchers from the Center for Global Discovery and Conservation Science discovered aircraft-measured spectral differences in the foliar

traits of trees that would later develop visible signs of ROD. This finding suggests that their unique aircraft mapping system may provide early detection of trees affected by the pathogen.

"We used repeat laser-guided imaging spectroscopy of forests on Hawai'i Island collected by the ASU Global Airborne Observatory to derive maps of foliar characteristics previously found to be important in distinguishing between ROD-infected and healthy 'Ōhi'a canopies," said Erin Weingarten, lead author, and now a PhD student at Colorado State University. "Data from these maps were used to develop a prognostic indicator of tree stress prior to the visible onset of browning."

The ASU Global Airborne Observatory, or "lab in the sky," mapped the two forest canopies from 2018 to 2019. Over the course of the year, one group of trees remained green. The other group changed from green to brown due to the onset of ROD symptoms. The team then assessed and compared spectral data of each group in 2018 for the foliar traits, or properties, of the leaves that have been linked to ROD. After analysis, the researchers observed key spectral differences in the leaf traits before the canopy turned brown. *https://news.asu.edu*

Remote sensing satellite lifted successfully into orbit

China successfully sends a new remote sensing satellite of the Yaogan 34 series into space from the Jiuquan Satellite Launch Center in Northwest China at 3:09 pm on March 17, 2022.

The satellite will team up with its predecessor, the Yaogan 34-01, which has been in operation for nearly 11 months *www.chinadaily.com*

MOSTI helps NADMA to analyse soil movement

The Ministry of Science, Technology and Innovation (MOSTI), Malaysia is helping the National Disaster Management

Agency (NADMA) to analyse soil movement at Taman Bukit Permai 2, Ampang using space remote sensing.

MOSTI deputy minister Datuk Ahmad Amzad Hashim said the analysis was carried out using the technology developed by the Malaysian Space Agency (MYSA).

He said seven types of information obtained from remote sensing and satellite images could provide early data in connection with soil movements, which could help in addressing landslide-related risks posed by such incidents that occurred at the housing area. *www.nst.com*

Introducing the US Commercial Remote Sensing Legislation

House Science, Space, and Technology Committee Ranking Member Frank Lucas (R-OK) and Representative Ed Perlmutter (D-CO) announced the introduction of H.R. 6845, the Commercial Remote Sensing Amendment Act, to support commercial remote sensing activities in the U.S. The bill renews an expired requirement for the Department of Commerce to send an annual report to Congress on the status of commercial remote sensing applications, regulations, and adjudications.

"Remote sensing has become a crucial tool allowing us to improve crop production, weather forecasting, and emergency responses to natural disasters," Lucas said. "The technology is constantly evolving, and the commercial remote sensing industry is seeing tremendous growth. To effectively support and manage commercial remote sensing activities, Congress needs timely and comprehensive reports from the Department of Commerce so we can evaluate the state of the industry and how regulations are affecting its growth. I appreciate Representative Perlmutter's support of this legislation, and I look forward to working with him to pass this into law."

"The American remote sensing industry leads the world in developing new technologies and capabilities to better

understand what's happening here on Earth and make informed decisions," Perlmutter said. "Congress has a responsibility to effectively encourage and support the remote sensing industry, and this legislation will provide the information and data necessary to ensure continued growth and global leadership. I look forward to working with Ranking Member Lucas and my colleagues on this important bill." *https://republicans-science.house.gov*

Copernicus Land Monitoring Service

The European Environment Agency (EEA) recently awarded a contract to a consortium under the lead of GAF with the partners GeoVille and VITO to implement the new High-Resolution Layer (HRL) Vegetated Land Cover Characteristics (VLCC), as part of the pan-European Copernicus Land Monitoring Service (CLMS). Its rich product portfolio will ensure both the continuation and evolution of successful precursor HRLs, such as Forest and Grassland, and the establishment of new HRL products focusing on crops and agricultural practises. The implementation of HRL VLCC will happen with funding by the European Union.

The HRL VLCC will comprise pan-European mapping of several new agriculture-related CLMS products such as annual crop types, agricultural cropping patterns and grassland mowing until the year 2023, while ensuring consistency with the grassland and forest products. The VLCC will form part of the pan-European component of the Copernicus Land Monitoring Service (CLMS), making regular large-scale information products available to a broad user community from European public bodies, to EEA member and cooperating countries, regional environmental authorities, research and academia as well as the value-adding sector. It will provide support for various environmental policies and make a significant contribution to assessing Europe's current environmental status and monitoring changes over time. *www.pressebox.de* ◪

EASA publishes SIB to warn of intermittent GNSS outages near Ukraine conflict areas

The European Union Aviation Safety Agency has published a Safety Information Bulletin (SIB) warning of the increased probability of problems with GNSS in the current context of the Russian invasion of Ukraine.

The SIB proposes mitigation actions to be taken by the National Aviation Authorities, Air Navigation Service Providers and air operators to address the issue that spoofing and/or jamming has intensified in geographical areas surrounding the conflict zone and in other areas. *www.easa.europa.eu*

Ready to navigate into the future – Galileo 2nd generation satellites

Airbus has successfully completed the Preliminary Design Review (PDR) for its system concept for the second generation Galileo navigation satellites. During this important milestone, Airbus' proposed preliminary design and the customer's system requirements have been fully reviewed and agreed. This paves the way for further verification, acceptance and qualification at equipment and module level. Verification at payload level is already in full swing, with the Critical Design Review (CDR) for the satellite structure also due shortly.

In parallel, the Airbus site in Friedrichshafen, on Lake Constance, is preparing for an industrialised production line for currently six second-generation Galileo satellites. The satellite integration centre, is being completely upgraded to meet current and future requirements for efficient, environmentally friendly, safe and secure production for the Galileo 2nd generation satellitesthat are planned to be launched in 2024. The world of navigation is changing, driven by rapidly emerging and changing user needs (availability and reliability), a growing number of security threats (jamming and spoofing) and the evolution of other navigation systems. The new batch of Galileo spacecraft built by Airbus is the

answer to this changing context. It will make the Galileo service more accurate, secure and dependable, and adaptable over its lifetime spanning two decades.

Weighing around 2.3 tons, each satellite is designed to operate for about 15 years. The state-of-the-art and all-electric medium-Earth orbit (MEO) platform from Airbus, reuses flight proven building blocks from our Telecoms and Earth Observation programmes, taking advantage of a unique combination of heritage and in orbit experience. The flexible and modular navigation payload solution with future growth capability is also based on telecom elements for signal generation. *www.airbus.com*

HawkEye 360 detects GPS interference in Ukraine

HawkEye 360 Inc. has announced the capability to detect and geolocate GPS interference, with analysis of data over Ukraine revealing extensive GPS interference activity. HawkEye 360 uses satellites to monitor radio frequency signals for interference that might threaten military and civil navigation applications. The capability was tested last year in a variety of exercises and is currently available as part of HawkEye 360's RFGeo signal product catalogue. *www.he360.com*

i83 IMU–RTK GNSS receiver by CHC Navigation

CHC Navigation (CHCNAV) today announced the availability of the i83 GNSS receiver, a new and innovative addition to its premium GNSS receiver series for surveying, mapping and construction professionals. It is powered by 1408-channel multi-band GNSS, the latest iStar technology, and a calibration-free, high-end IMU sensor for faster and reliable field GNSS surveying. The receiver combines GNSS and IMU into one single receiver to provide optimal automatic pole tilt compensation that requires no calibration and is fully immune to magnetic interference. Operators just need to focus on their tasks and no longer need to level their pole vertically. *chcnav.com* ◣

GMV guarantees PAZ satellite services

GMV has signed a new contract with INTA (Instituto Nacional de Técnica Aeroespacial) for the corrective maintenance of the main elements of its ground segment. The Spanish Paz satellite, with an estimated useful life of seven years, is a dual-use (civil/military) Earth observation satellite in orbit at an altitude of 514 kilometers over the poles and designed for surveillance applications, high-resolution mapping, border control, tactical support in foreign missions, crisis and risk management, natural disaster assessment, environmental control, and maritime environment monitoring.

VERIPOS expands SPAN GNSS+INS portfolio

VERIPOS expands its proven inertial solution SPAN GNSS+INS technology from NovAtel, to dynamic positioning (DP) applications and vessels. SPAN technology delivers a deeply coupled GNSS and inertial navigation system (INS) that provides robust, reliable and continuous centimetre-level positioning for operators to maintain safety and maximize uptime. With a GNSS+INS solution, DP vessels can bridge outages in GNSS tracking and through short periods of radio frequency interference, jamming or spoofing. *https://veripos.com*

Septentrio GNSS receivers to support the CLAS

Septentrio has launched three new products: mosaic-CLAS, AsteRx-m3 CLAS and AsteRx SB3 CLAS, which support Japan's high-accuracy Centimeter Level Augmentation Service (CLAS). These GNSS receivers support CLAS on a single device, thanks to the latest GNSS technology which receives the L6 signal, which transmits high-accuracy corrections from Japan's QZSS constellation. This technology was developed in close cooperation with CORE, a leading integrator of high-accuracy positioning technology and services in Japan. septentrio.com

Harxon Smart Antenna TS112 PRO

Harxon has introduced Smart Antenna TS112 PRO to provide scalable and reliable positioning solutions for severe environments with uneven grounds, underground cables, etc. It is designed with the most up-to-date GNSS technology provided by Harxon and GNSS module provided by Hexagon | NovAtel. Harxon's X-Survey™ OEM GNSS antenna and Hexagon | NovAtel's OEM GNSS module combine to offer centimeter-level positioning accuracy with excellent interference mitigation performance for farming fields and wild environments. *harxon.com*

Locating Shackleton's historic Endurance using technology by Sonardyne

After more than 100 years lost more than 3,000 m underneath sea ice in the Antarctic's Weddell Sea, the almost fully intact wreck of Ernest Shackleton's Endurance has been found, supported with underwater navigation and positioning technology from Sonardyne.

The pioneering search, launched in February this year, saw the Endurance22 team deploy Saab Seaeye Sabertooth hybrid autonomous underwater vehicles (AUVs) from the icebreaking polar supply and research shipS.A. Agulhas II. During their hunt of the seabed, close to where the 1914-1917 expedition came to its end, these underwater robots used Sonardyne's SPRINT-Nav hybrid acoustic-inertial navigation system (INS) technology navigate their search routes. They also used Sonardyne's AvTrak 6 tracking and telemetry transceiver, to send commands and position updates from a Ranger 2 Ultra-Short BaseLine (USBL) system, also from Sonardyne, onboard the S.A. Agulhas II. *https://endurance22.org*

Eos Laser Mapping for Android by Eos Positioning

Eos Positioning Systems has released its popular Eos Laser Mapping™ for ArcGIS solution on Android devices. Previously the free solution, which allows mobile

crews to capture asset locations from a distance with survey-grade accuracy, was available only on iOS. The solution combines technology from GIS provider Esri, laser rangefinders from Laser Tech (LTI), and Eos' own popular Arrow Series® GNSS receivers. The new release on Android currently supports three workflows, or mapping methodologies: Standard Laser Offset (sometimes called Range-Azimuth), Range-Range (or Range-Intersect), and Range-Backsight (a total station-like method).

SkyDeck– A software platform for delivering DaaS

Asteria Aerospace has launched its end-to-end drone operations platform – SkyDeck. It is a cloud-based software platform to deliver a DaaS solution for multiple industry verticals such as agriculture, surveying, industrial inspections, and surveillance and security. *https://asteria.co.in*

ORKID partnership with Unifly

ORKID has partnered with Unifly, UTM technology provider, in a series of test operations. These flight operations will mark an especially important milestone in the certification process required by Aeronáutica Civil, so that ORKID can continue to conduct recurrent commercial flight operations in the near future. *www.orkid.tech*

Antenova's 'Pharaoh' 4G antenna

Antenova Ltd has halved the footprint of its 4G cellular antennas with its latest offering, the Pharaoh SMD antenna. Designed for small PCBs, the antenna (P/N SR4L073) covers all 4G frequencies: 698 – 824 MHz, 824-960 MHz, 1710-2170 MHz, 2300-2400 MHz and 2500-2690 MHz.

World's smallest Iridium antenna

Helix Geospace has launched the world's smallest Iridium antenna, which can operate safely near the human head with minimal performance degradation. At only 37mm long and 13.5mm diameter, the HXDC1600 antenna family that meets the Iridium satellite data network's voice and short-burst data (SBD) requirements. The new Iridium antenna will enable satellite phones to be built at close to the size and cost of a normal cellular mobile phone.

SingularXYZ Launched SAgro100 Automated Steering System

SingularXYZ recently released SAgro100 automated steering system for precision agriculture, improving agricultural resource utilization and productivity. The integrated full-constellation tracking GNSS module and sensitive electric motor enable the SAgro100 to deliver centimeter auto-steering accuracy. The 2.5cm pass-to-pass accuracy largely improves the utilization of land and other resources, while freeing farmers' hands. ◺

◺ MARK YOUR CALENDAR

May 2022

GEO Business 2022
18-19 May
London, UK
www.geobusinessshow.com

June 2022

8th International Conference on Cartography and GIS
20 to 25 June 2022
Nessebar, Bulgaria
https://iccgis2020.cartography–gis.com

July 2022

IGARSS 2022 (hybrid form)
17-22 July 2022
Kuala Lumpur, Malaysia
https://igarss2022.org

September 2022

Commercial UAV Expo Americas
6-8 September 2022
Las Vegas, USA
www.expouav.com

ION GNSS+ 2022
19-23 September
Denver, CO, USA
www.ion.org/gnss/index.cfm

October 2022

Intergeo Hybrid
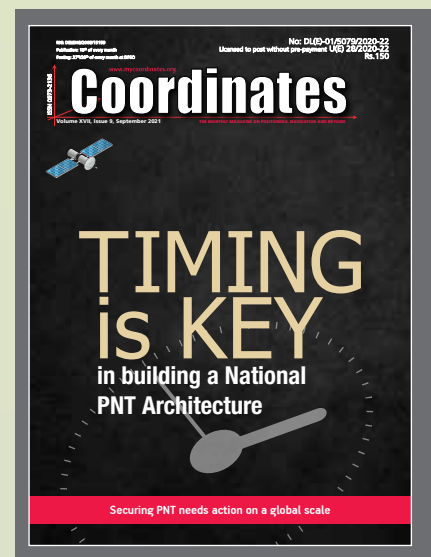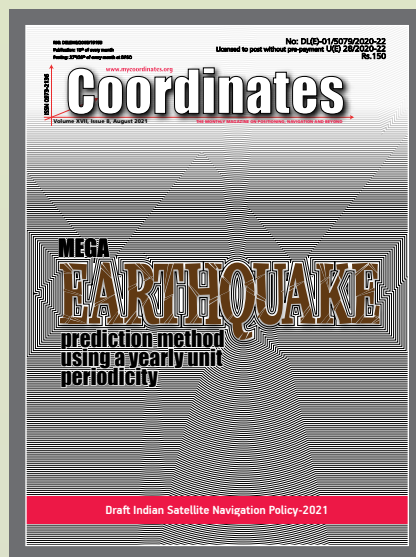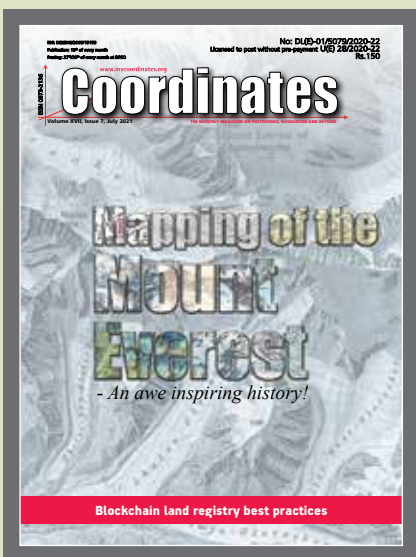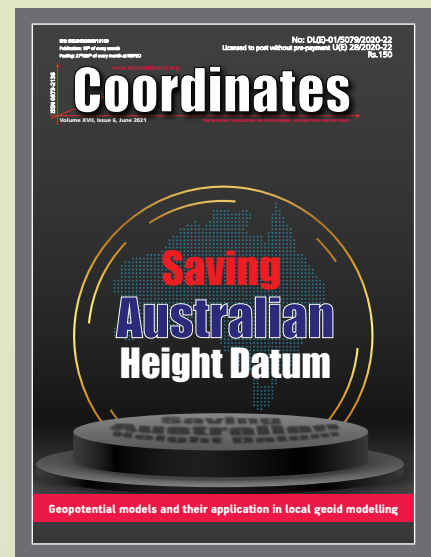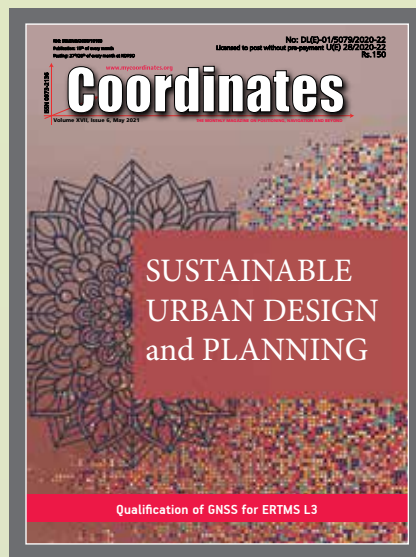18-20 October 2022
Essen, Germany
www.intergeo.de

November 2022

Trimble Dimensions+
7–9 November 2022
Las Vegas, USA
https://dimensions.trimble.com
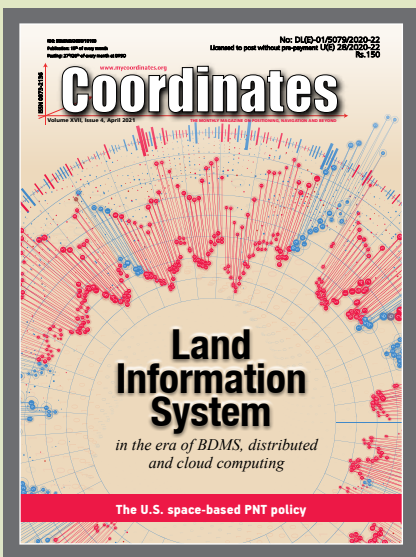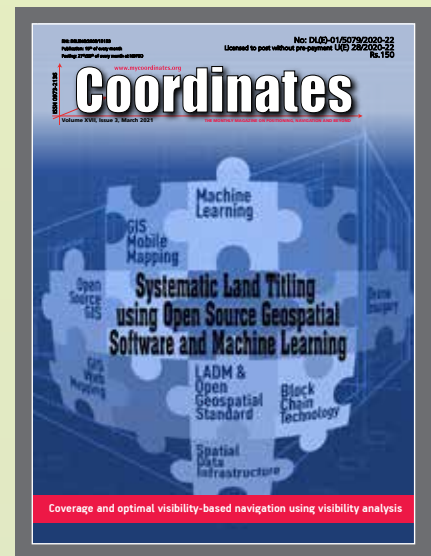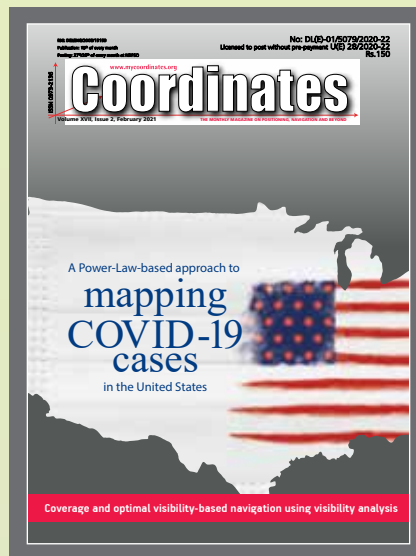
"The monthly magazine on Positioning, Navigation and Beyond"
Download your copy of Coordinates at www.mycoordinates.org